Blocking the EGFR/p38/NF-κB Signal Pathway Alleviates Disruption of BSCB and Subsequent Inflammation After Spinal Cord Injury

Zai-Wang Li (lizaiwang123@126.com)
Shenzhen People's Hospital https://orcid.org/0000-0003-3738-3917
Jing-Jing Zhao
Nanjing Medical University Affiliated Wuxi People's Hospital: Wuxi People's Hospital
Su-Ya Li
Wuxi People's Hospital of Nanjing Medical University
Ting-Ting Cao
Yancheng First People's Hospital
Yi Wang
University of Traditional Chinese Medicine
Yi Guo
Shenzhen People's Hospital
Guang-Jun Xi
Wuxi People's Hospital of Nanjing Medical University

Research

Keywords: EGFR/p38/NF-κB, BSCB, spinal cord injury, subsequent inflammation

Posted Date: January 5th, 2021

DOI: https://doi.org/10.21203/rs.3.rs-138257/v1

Abstract

Background:

Epidermal growth factor receptor (EGFR) activation may play an important role in blood spinal cord barrier (BSCB) disruption and secondary injury after SCI as it is significantly upregulated in the astrocytes (AS) and microvascular endothelial cells (MEC), which are the main component of cells in BSCB. EGFR inhibition alleviates the disruption of BSCB and improves the functional recovery in rats following spinal cord injury (SCI). However, the biological mechanisms underlying EGFR activation mediating secondary damage after SCI remain unclear.

Methods:

An *in vitro* model of Oxygen and glucose deprivation/reoxygenation (OGD/R) induced BSCB damage and *in vivo* rat SCI model was employed to define the role of EGFR activation and its induced inflammatory injury during this pathological process in AS and MEC. AS and MEC were exposed to EGFR or p38 MAPK up-regulation in the presence and absence of EGFR inhibitor, p38 MAPK inhibitor, NF-κB inhibitor, and/or appropriate shRNA. RT-PCR, ELISA and western blotting were used for mRNA and protein expression analyses of TNF-α, iNOS, COX-2 and IL-1β. Immunohistochemical staining and confocal microscopy were used to demonstrate cellular EGFR activation and to investigate the expression of tight junction (TJ) protein (ZO-1 and occludin). Measurement of transendothelial electrical resistance (TEER) and transendothelial FITC-dextran permeability were used to measure permeability of BSCB *in vitro*, while Evans blue dye extravasation test and evaluation spinal cord edema were used to detect permeability of BSCB *in vivo*.

Results:

The expression of pEGFR was significantly increased in BSCB component cells (AS and MEC) after SCI and BSCB damage model. EGFR activation induced inflammation injury by upregulating the expression of TNF-α, iNOS, COX-2, and IL-1β and BSCB disruption with loss of TJ protein by downregulating the expression of ZO-1 and occludin in BSCB damage model and SCI rats. Moreover, EGFR or p38 activation leads to NF-κB nuclear translocation in primary AS and MEC after OGD/R. The EGFR inhibitor as well as shRNA against EGFR markedly attenuated pro-inflammatory factor excessive producing and loss of TJ protein, and activation of the EGFR/p38/NF-κB pathway. While, EGFR overexpression significantly increased the expression of TNF-α, iNOS, COX-2, and IL-1β and decrease the expression of ZO-1 and occludin, inducing activation of the EGFR/p38/NF-κB pathway in both AS and MEC.

Conclusion:

This study strongly suggests that EGFR activation in BSCB component cells after SCI and BSCB damage model mediates both upregulation of pro-inflammation expression and downregulation of TJ protein downregulation via the EGFR/p38/NF-κB pathway. These findings contribute to a better understanding of

the biological mechanisms underlying BSCB disruption and secondary injury following SCI mediating by EGFR activation.

Introduction

Spinal cord injury (SCI) can cause severe neurological functional deficits, which can lead to serious adverse effects in quality of life of patients with SCI, placing a heavy burden on families and society[1]. Neurological functional deficit following SCI arises from initial primary mechanical injury following by a subsequent secondary injury[2], which has a close relationship with blood spinal cord barrier (BSCB) disruption[3, 4]. Microvascular endothelial cells (MEC) injury in traumatic mechanical violence causes damage of the BSCB[4], which leads to a mass of peripheral inflammatory cells and pro-inflammatory cytokines that invade the spinal cord nervous tissue[5]. Dual effects of traumatic mechanical violence and inflammation trigger activation of microglia and astrocytes and incur reactive gliosis[6], which escalates inflammatory reaction, eventually causing neighboring neuron loss and demyelination[6–8]. Above all, inflammation following SCI can also cause BSCB damage of neighboring intact spinal cord tissue, which induces a new round of peripheral inflammatory cells and factors that invade the spinal cord tissue and activate a cascade of secondary damage processes (the damage positive feedback)[6, 8]. In short, the pathogenesis of secondary injury after SCI is closely related to the damage positive feedback, which is formed by damage of BSCB and the ensuing inflammatory injury evoking neural tissue damage[8, 9]. The destruction of BSCB plays a key role in the pathogenesis of secondary injury after SCI [8]. Therefore, protecting the structural and functional integrity of BSCB after SCI is crucial to control secondary damage and reconstruct the spinal cord neural tissue microenvironment homeostasis after SCI[8, 10, 11].

Recent studies have demonstrated that epidermal growth factor receptor (EGFR) signal path is involved in functional regulation of the cell barrier[12, 13]. Microvascular damage, pulmonary injury and abnormal changes of intestinal intima permeability are all associated with EGFR activation[13, 14]. Several studies have demonstrated activated EGFR occurrence in astrocytes, microglia, and microvascular endothelial cells during central nervous system disorders including SCI[15–18]. Meanwhile, inhibiting EGFR activation may ameliorate BSCB damage and improve neurological deficit symptoms[19, 20]. Hence, EGFR activation might play a key role in BSCB damage and secondary injury after SCI[8, 14, 21]. However, the specific mechanism of BSCB damage and secondary spinal cord injury caused by EGFR activation after SCI is still unclear. In this study, the relationship and underline mechanism of signal pathway between EGFR activation, the expression of pro-inflammatory factors and tight junction protein in AS and SCMEC after SCI was investigated. Moreover, the potential molecular signal path involving EGFR activation causing BSCB damage and secondary injury after SCI was explored.

Material And Methods

2.1 Animals and surgery

Animal procedures were performed in strict accordance with protocols approved by the Institutional Animal Care and Use Committee at Jinan University. Adult female Sprague-Dawley rats (weight 220 to 250 g) were randomly classified into SCI and sham-operated groups, housed under conditions of constant temperature (25±1°C) and humidity (55±5%), with a 12 h light-dark cycle. A T10 contusion injury was produced by a trained technician as described in previous studies[17, 19]. Briefly, the rats were anesthetized by intraperitoneal (ip) injection of ketamine (80 mg/kg) and xylazine (10 mg/kg). Once rats were confirmed to be unconscious by toe-pinch, a laminectomy was performed at vertebral level T10 on the back of the rat. After immobilizing the spine stereotaxically, a weight-drop injury was induced by using a standardized instrument (New York University Impactor) releasing a weight (10 g, rod diameter of 2 mm) from a height of 12.5 mm on the exposed dura of the spinal cord at thoracic level T10, inflicting a moderate contusion injury. The rats were randomly assigned to either PD168393 or vehicle treatment groups. Immediately following SCI, an osmotic mini pump (Alzet Corp., Palo Alto, CA, USA) placed between the shoulder blades was connected to a 32 gauge catheter and the catheter tip was positioned subdurally on the dorsal side of the spinal cord over the center of the injury through a small hole in the dura mater. In the PD168393-treated group, the osmotic pump was filled with 2 mM PD168393 (Sigma-Aldrich, St. Louis, MO, USA) dissolved in 5% DMSO, then the rats were micro-infused immediately after pump placement at a rate of 0.5 μL/h for 14 days[17]. The Control animal were given 5% DMSO. Lastly, the back muscles and skin layers were then sutured and animals were returned to their original warm incubators for recovery. After 14 days, the pumps were removed and then the wound was closed with surgical suture. The Sham-operated animals underwent laminectomy alone. Bladders were expressed twice daily until urinary incontinence disappeared.

2.2 Rat Primary spinal cord mixed glial cells (astrocytes and microglia) culture

Spinal cord mixed glial cells (astrocytes and microglia) were derived from neonatal rat spinal cord as described in our previous study [8, 22]. Briefly, the rat pups at postnatal day 0~2 were sacrificed by cervical dislocation and disinfected with 75% alcohol for about 3~5 min, followed by dissection and separation from the whole spinal column via ophthalmological instruments. The spinal cord was discharged by injecting cold D-Hank's solution into the spinal column and then the meninges were removed. After that, the extracted spinal cord was minced, digested in PBS (pH = 7.4) containing 0.25% collagenase (Sigma-Aldrich, St. Louis, MO, USA) for 15 min at 37°C, filtered through a 70 μm cell strainer, and centrifuged at 1000 rpm for 5 min. Subsequently, the resulting pellet was re-suspended and cells were plated in culture flasks at a density of 1 × 106 cells/ mL and maintained in culture at 37℃ with 5% CO2 in DMEM supplemented with 10% FBS (Hyclone) and 0.5 mg/mL penicillin/streptomycin. After 48 or 72 h, the medium was changed every 3 days thereafter. After a total of 21 days in culture, the mixed glia were passaged with 0.25% trypsin, re-suspended in astrocytic freezing medium (DMEM, 10% FBS, 10% DMSO) at a concentration of 2~3 × 106 cells/mL, and frozen at a rate of 1°C/min at −80°C using a Nalgene freezing container.

2.3 Rat primary spinal cord astrocytes culture

Spinal cord astrocytes from neonatal rat spinal cord were prepared according to an established protocol[23]. Briefly, pups at postnatal day 0–2 were decapitated following sterilization of the body with 75% ethanol. The spinal cords of rat pups were isolated following painless sacrifice. Meninges were removed and the spinal cord was minced, digested in 0.25% collagenase in PBS (pH 7.4), for 10 to 20 minutes at 37°C and then passed through a 70 μm nylon mesh Digested tissues were centrifuged at 1,000 rpm for 2 minutes, then the supernatant removed carefully, the tissue pellet re-suspended, cells were plated on culture flasks at a density of 1~3× 106 /mL and maintained in DMEM supplemented with 10% FBS (Hyclone) and 0.5 mg/mL penicillin/streptomycin at 37°C with 5% CO2. Cell culture medium was changed 2 days after plating and every 3 days thereafter until astrocytes reached confluence. During week 2 in vitro, non-astroglial cells were removed by mildly shaking. The astrocytes remaining in culture medium were identified by immunostaining with anti-GFAP. Approximately 95% of the cells were immunopositive for GFAP. All experiments were performed on spinal cord astrocytes maintained for two to three weeks in culture.

2.4 Rat primary spinal cord microvascular endothelial cells culture

Primary spinal cord microvascular endothelial cells (MEC) were obtained from rats pups at postnatal day 0~2, and the isolation and culture of MEC was performed according to the protocol previously described[8, 24]. Briefly, spinal cords were isolated following painless sacrifice and then large vessels and meninges were eliminated successively. Then, the dissected spinal cord tissues were finely minced into small pieces using iris scissors in cold DMEM/F-12 and manually homogenized on ice for several rounds in a glass homogenizer. Subsequently, the homogenates were digested in pre-warmed ACCUTASE in a shaker for 30 min at 37°C, centrifuged for 5 min at 2000 rpm. Solid fraction pellets were then re-suspended in 22% bovine serum albumin, followed by centrifugation for 15 min at 4000 rpm. The upper myelin layer was aspirated and washed 3 times with HBSS, followed by digestion with pre-warmed ACCUTASE in a shaker at 37 °C for 30 min. Then, the digested tissues were centrifuged at 2000 rpm for 5 min at 4°C and re-suspensed in MEC culture medium [DMEM/F12, supplemented with 10% FBS, 0.5 mg/mL penicillin/streptomycin and 30 ng/mL endothelial cell growth factor (PeproTech)]. Finally, cells were plated on poly-D-lysine-coated culture flasks at a density of 1 × 104 cells/mL and cultured at 37°C in 5% CO2. The MEC were identified by immunofluorescence labeling with anti-CD31. The rate of MEC (CD31-positive) was greater than 95%.

2.5 BSCB damage model *in vitro*

A BSCB damage model in vitro was produced as described in a previous study[8]. Briefly, re-suspended rat spinal cord MEC cells were seeded on the upper chambers (inserts) of a 12-well Transwell system (polyester membrane, 12 mm diameter, 0.4 μm pore size, Corning Costar, HighWycombe, UK) at a concentration of approximately 5 × 104 cells/mL and 400 μL/well. Then, the upper chambers with MEC were added onto the bottom chambers of the transwell system with pre-seeded spinal cord mixed glial cells and co-cultured in DMEM/MVGS culture medium for 7~14 days with media changes occurring every 3 days.

Oxygen and glucose deprivation/reoxygenation (OGD/R) treatment was applied to the above-mentioned cells in the Transwell system in vitro to mimic BSCB damage in vivo. After three washes with PBS, the cells were cultured with glucose-free DMEM/F12 in a hypoxia incubator (oxygen concentration ≤1%) equilibrated with 95% N2 and 5% CO2 at 37℃ for 3 h in order to induce hypoxic damage to the in vitro BSCB model. After OGD exposure, cells were returned to normal culture in glucose-containing DMEM/F12 under normoxic conditions for reoxygenation. As a control group, cells were washed with glucose-containing DMEM/F12 three times, and then cultured in glucose-containing DMEM/F12 under normoxic conditions at an oxygen concentration of 20%.

2.6 Cell treatment

2.6.1 Agonists and inhibitors for EGFR and p38 MAPK in AS and MEC

Cells were seeded at 1 × 105 cells/cm2 onto glass coverslips in 24-well culture plates. Agonists for EGFR and p38 MAPK were given following OGD treatment, with final concentrations at 5nM (EGF) (Sigma-Aldrich, St. Louis, MO, USA)or 10mM (Isoprenaline) (MCE). Inhibitors for EGFR and p38 MAPK were given following OGD treatment, with final concentrations at 1 nM (PD168393) (Millipore) or 10μM (SB203580) (Sigma-Aldrich, St. Louis, MO, USA). The solvent served as the control treatment. Supernatants were collected for ELISA, while cells were fixed by methanol (−20°C, 15 min) for staining at various harvesting time points.

2.6.2. Overexpressing of EGFR and p38 MAPK in AS and MECs

Cells were grown to confluence on 100cm2 culture plates in Dulbecco's modified Eagle's medium with 4.5 g/L glucose, 3.7 g/L sodium bicarbonate, 4 mM glutamine, 10% fetal bovine serum, 100 U/mL penicillin, and 100 g/mL streptomycin. Cells were transfected with lentivirus vector （1×109TU/ml） containing the cDNA fragments encoding the full-length rattus EGFR and p38 MAPK protein. The target gene overexpresses lentivirus was purchased from Genechem (Shanghai, China). Cells transfected the empty with expression vector served as controls. Transfection efficiency was monitored by fluorescence microscopy.

2.6.3 EGFR and p38 MAPK siRNA transfection in AS and MECs

A lentiviral EGFR short hairpin RNA (shRNA) was purchased from Genechem (Shanghai, China). A scrambled shRNA was included as a negative control. To knockdown endogenous EGFR, and p38 MAPK, cells were transfected with Infection enhancer fluid HitransG A (Genechem, Shanghai, China) plus shRNA according to the manufacturer recommendations. In general, cell suspensions were prepared as a density of 3~5 × 10^4 cells/mL with complete medium, 2mL cell suspension was added to each well of a six-well plate (bottom area of each well is 10 cm^2). Cells were cultured in a humidified incubator containing 95% air and 5% CO2 at 37°C for 16~24h, with regular media changes. Two uL shRNA (2×10^9TU/mL) in the medium containing 40uL infection enhancement solution HitransGA was then added to each well,

cultured for 6~8hours, and then replaced with conventional medium. Transfection efficiency was monitored by fluorescence microscopy after transfection for 72 h.

2.7 Immunocytochemistry staining of rat spinal cord sections

Rats in the sham, vehicle, and PD168393-treated injury groups were sacrificed 3 days post-injury for GFAP, CD31, and pEGFR double staining and sacrificed at days seven post-injury for ZO-1, Onccludin and CD31 staining (n=5 for each time points). The tissues were dissected and processed as previously described[17, 19]. Briefly, the rats were transcardially perfused with saline, followed by ice-cold 4% paraformaldehyde. After harvesting the 15mm length spinal cord samples centered on the injury site, the spinal cord segments were embedded in Optimum Cutting Temperature Compound (Sakura, USA), rapidly frozen in nitrogen-cooled isopentane, and stored at -80°C until time of processing. Spinal cord tissue blocks were cut horizontally at a thickness of 10 μm. Sections were mounted on poly-L-lysine-coated glass slides and stored at −20°C until further processed. Sections were then washed in PBS buffer solution and incubated with blocking solution containing 0.3% Triton-x and 5% normal goat serum in PBS at 37℃ for 1 hour. Immunofluorescence sections were treated with respectively with a combination of two primary antibodies: mouse anti-GFAP (1:400; Sigma-Aldrich, St. Louis, MO, USA) and rabbit anti-pEGFR (1:300; Sigma-Aldrich, St. Louis, MO, USA), rabbit anti-GFAP (1:300; Sigma-Aldrich, St. Louis, MO, USA) and mouse anti-CD31 (1:400; Sigma-Aldrich, St. Louis, MO, USA), rabbit anti-ZO-1 (1:200; Sigma-Aldrich, St. Louis, MO, USA) and mouse anti-CD31 (1:400; Sigma-Aldrich, St. Louis, MO, USA), rabbit anti-occludin (1:200; Sigma-Aldrich, St. Louis, MO, USA) and mouse anti-CD31 (1:400; Sigma-Aldrich, St. Louis, MO, USA) overnight at 4°C. After PBS washing, the sections for double-labelling immunofluorescence were incubated in a mixture of two secondary antibodies: Cy3-conjugated goat anti-rabbit IgG anti-body (1:300; Jackson ImmunoResearch, West Grove, PA, USA) and FITC-conjugated goat anti-mouse IgG antibody (1:300; Jackson ImmunoResearch, West Grove, PA, USA) or Cy3-conjugated goat anti-mouse IgG antibody (1:300; Jackson ImmunoResearch, West Grove, PA, USA) and FITC-conjugated goat anti-rabbit IgG antibody (1:300; Jackson ImmunoResearch, West Grove, PA, USA) for 1 hour at room temperature and stained with DAPI. Finally, the slides were washed twice in PBS and cover slips were mounted on slides using antifade medium (Sigma). Sections were observed under an Olympus BX-51 light microscope (Olympus, Tokyo, Japan) or a confocal laser-scanning microscopy (TCS SP8, Leica) and analyzed with Image-Pro Plus analysis software (Media Cybernetics, Inc., Silver Spring, MD, USA).

2.8 Western blotting analysis

Animals in the sham, injury, and PD168393-treated groups were deeply anesthetized and sacrificed at days 3, 7, and14 post-injury (n = 3 in each group for each time point). A 15 mm length spinal cord containing the injury epicenter was quickly removed for protein semiquantitative analysis in each group. For cell culture experiments, cells were harvested at 12 h of reoxygenation following OGD. And the Protein extracts were prepared and Western blotting was performed as described previously[17, 19]. Samples containing an equal amount of total proteins were loaded on SDS-PAGE (10% for EGFR/pEGFR; 12% for other proteins). The electrophoresed proteins were transferred onto nitrocellulose membranes (300 mA,

four hours for EGFR/pEGFR; 250 mA, two hours for others). After being blocked by incubation with Tris-buffered salina containing 0.1% Tween 20, 2% BSA, and 5% nonfat dry milk, the membranes were incubated overnight at 4°C with primary antibodies diluted in blocking buffer as follows:. monoclonal mouse anti-GFAP (1:1,000; Neomarkers, Fremont, CA, USA) for astrocytes, polyclonal rabbit anti-CD31 (1:500; Santa Cruz Biotechnology, Santa Cruz, CA, USA) for microvascular endothelial cells, polyclonal rabbit anti-pEGFR (1:500; Santa Cruz Biotechnology, Santa Cruz, CA, USA), polyclonal rabbit anti-EGFR (1:500; Santa Cruz Biotechnology, Santa Cruz, CA, USA), rabbit anti-ZO-1 (1:200; Sigma-Aldrich, St. Louis, MO, USA), rabbit anti-occludin (1:200; Sigma-Aldrich, St. Louis, MO, USA) , rabbit anti-COX-2(1:300 Invitrogen, USA), rabbit anti-iNOS (1:300 Invitrogen, USA), rabbit anti-IL1β(1:300 Invitrogen, USA), rabbit anti-TNFα (1:300 Invitrogen, USA), mouse anti-p65 (1:2000; Abcam, UK), mouse anti-p38 (1:2000; Abcam, UK), rabbit anti-β-Tubulin, mouse anti-Histone3 (1:2000; Abcam, UK), mouse anti-GAPDH(1:2000; Abcam, UK), or rabbit anti-β-actin (1:2,000; Neomarkers, Fremont, CA, USA) as a loading control. After washing the membranes with TBS containing 0.1% Tween 20, the blots were incubated with horseradish peroxidase-conjugated anti-mouse or anti-rabbit IgG (1:2,000; Neomarkers, Fremont, CA, USA) at room temperature for 1 hour and visualized with an enhanced chemiluminescence (ECL) system (Thermo Fisher Scientific Inc., USA). The membranes were scanned at 600 dpi, and digital images were quantitatively analyzed by a Kodak Digital Science 1D system. The optical density (OD) of the blots was semiquantified and expressed as the ratio of OD of the tested proteins to that of loading control (β-actin, β-Tubulin, GAPDH or Histone 3).

2.9 Reverse transcriptase-polymerase chain reaction (RT-PCR)

Rats in sham, injury, and PD168393-treated groups were deeply anesthetized and sacrificed at day 3 post-injury (n = 3 in each group). The 15 mm length spinal cord sample centered on the injury site was quickly separated, immediately frozen with dry ice, and stored at -80 °C until use. Total RNA was extracted from spinal cord segments and the cultured cells using Trizol Reagent (Gibco, USA) according to the manufacturer's protocol. RNA was transcribed into single-stranded DNA using MMLV according to the manufacturer’s instructions (Invitrogen). PCRs for TNF-α, iNOS, COX-2, and IL-1β and GAPDH were performed using Taq PCR Master Mix kit (201443 Qiagen) on a Mastercycler gradient PCR (Eppendorf, Gene Company) using a protocol consisting of 94 °C for 2 min in 1 cycle and denaturation at 94 °C for 30 s, annealing at 55 °C for 30 s, and extension at 72 °C for 60 s in each of 35 cycles for GFAP and 25 cycles for GAPDH, respectively. The primers were as follows: for Cox-2：5’-CCA TGT CAA AAC CGT GGT GAA TG-3’ (sense) and 5’-ATG GGA GTT GGG CAG TCA TCA G-3’ (antisense); iNOS, 5’-CTC CAT GAC TCT CAG CAC AGA G-3’ (sense) and 5’-GCA CCG AAG ATA TCC TCA TGA T-3’ (antisense); IL-1β, 5’-GCA GCT ACC TAT GTC TTG CCC GTG-3’ (sense) and 5’-GTC GTT GCT TGT CTC TCC TTG TA-3’ (antisense); TNF-α, 5’-CCC AGA CCC TCA CAC TCA GAT-3’ (sense) and 5’-TTG TCC CTT GAA GAG AAC CTG-3’ (antisense). The PCR products were electrophoresed through a 1% agarose gel. Then Images were captured and the data processed using a Gene Genius Bio-Imaging system (Syngene) with GeneSnap and GeneTools software. Levels of mRNA were calculated as specific mRNA to GAPDH intensity ratios to determine the relative amount of the specific mRNA.

2.10 Measurement of pro-inflammatory factors by ELISA

The amount of pro-inflammatory factors (TNF-α, iNOS, COX-2, and IL-1β) was detected in the conditioned medium from each group using ELISA immunoassay kits according to a previous study [19]. Briefly, after constructing a standard curve, several dilutions of the test sample were assayed in duplicate for each protein using the appropriate kit. Plates were read using a VERSA max microplate reader (Molecular Devices, Sunnyvale, CA, USA) at a 450-nm wavelength with a reference wavelength of 570 nm. Regression analysis was then performed on standards and sample concentrations were determined with reference to the linear portion of the standard curve.

2.11 Evaluation of blood-spinal cord barrier disruption *in vitro*

2.11.1 Measurement of transendothelial electrical resistance (TEER)

Measurement of TEER was performed as previously described [8, 25]. The Transwell system, BSCB in virro, was treated with OGD for 3 h followed by re-oxygenation at 3 h, 6 h, 12 h, 24 h, and 48 h, respectively. TEER values in the OGD/R group and control group were measured by Millcell ERS-2 (Merk-Millipore) at each time point. In order to accurately calculate TEER (Ω×cm2), the electrical resistance across the insert membrane (blank resistance) was subtracted from the readings obtained on inserts with cells (sample resistance). This value was multiplied by the surface area of the insert (0.33 cm2).

2.11.2 Transendothelial FITC-dextran permeability evaluation

The experimental protocol of FITC-dextran permeability evaluation was described in detail in our previous studies [8, 26]. Following OGD/R treatment of the BSCB in vitro, FITC-dextran (1 mg/mL) in serum-free DMEM was added to the inserts of the Transwell system and incubated for 30 min at 37℃. FITC-dextran content accumulated in the bottom chamber of the Transwell system was subsequently quantified by transfer of 100 μL of every sample to a black walled-96 well plate for Envision fluorescence microplate assessment.

2.12 Evaluation of blood-spinal cord barrier disruption *in vivo*

2.12.1 Measurement of BSCB permeability by Evans blue dye extravasation

Permeability of the BSCB was assessed by Evans blue dye extravasation according to previous report[27] with minor modifications. Rats (n=6 in each group) were given a 2% EB saline solution (2mL/kg) by intravenous injection at day 3 after SCI, and then transcardially perfused with normal saline until colorless, transparent fluid flowed out of the right auricle after 2 h of EB circulation. A 15mm length of spinal cord surrounding the T10 injury site was extracted and homogenized in a 50% trichloroacetic acid solution, and cleared by centrifugation 18,000 G for 20 minutes at 4℃. A standard curve with Evans Blue dye (in formamide) was generated and fluorescence intensity was measured in supernatants (in duplicate) using a spectrophotometer (Thermo Fisher Scientific MultiSkan Go) with an excitation

wavelength of 620 nm and an emission wavelength of 680 nm. All measurements were converted to dye concentration per tissue weight(μg/g of tissue).

Half of the rats from all groups (n=5 in each group) received a cardiac perfusion with 4% paraformaldehyde after 2h of EB injection. Then 10 μm spinal cord sections were cut with a cryotome (Thermo Shandon). Exosmotic EB in spinal cord was observed using an Olympus bx-60 fluorescence microscope under 550 nm wavelength green light excitation.

2.12.2 Evaluation of spinal cord edema

The water content of the spinal cord can be used to evaluate of spinal cord edema[28]. Spinal cord samples from lesions were excised at day 3 post-injury and immediately weighed (wet weight). Afterwards, the Samples were incubated in a dryer for 24 h at 80℃ and then weighed again (dry weight). The water content of the spinal cord was measured using the following formula[29]: percentage of water = [1- (dry weight/wet weight)]×100.

2.13 Statistical analysis

Data are presented as mean ± standard deviation (SD). Statistically significant differences between data (defined as $P < 0.05$) were evaluated by Student's t-test or one-way analysis of variance (ANOVA) followed by Tukey's post hoc test. For comparison between groups over time, a multiple-measurement ANOVA was used.

Results

3.1 EGFR activation in AS and MEC and excessive astrogliosis following OGD/R in vitro

3.1.1 EGFR activation and excessive astrogliosis in AS following OGD/R in vitro

To examine whether EGFR activation in AS and excessive astrogliosis was a common phenomenon following OGD/R in BSCB model *in vitro*, double-immunofluorescent labeling for pEGFR and GFAP was performed at 12 h of reoxygenation following OGD 3 h. As shown in Fig. 1, there was nearly no co-localization of pEGFR and GFAP in the control group (Fig. 1A4), indicating that quiescent astrocytes did not exist with EGFR phosphorylation. However, in the OGD/R group, most of astrocytes showed increased phosphorylation of EGFR (Fig. 1B4). Furthermore, PD168393 (EGFR inhibitor) administration effectively inhibited EGFR phosphorylation from injury in AS (Fig. 1C4) and inhibited excessive astrogliosis following OGD/R in the BSCB model *in vitro* as well (Fig. 1D and E).

3.1.2 EGFR activation in MEC following OGD/R in vitro

To see if MEC have the same response to OGD/R the same experiment was performed using these cells. Co-localization of p-EGFR and CD31 were non-existent in the control group (Fig. 2A4), while co-localization of p-EGFR and CD31 was substantial in the injury group (Fig. 2B4). Interestingly, PD168393

administration effectively inhibited pEGFR immunoreactivity (Fig. 2C4) and the expression of pEGFR protein (Fig. 2D, E) in MEC following OGD/R in BSCB model in vitro. The results in Fig. 1 and Fig. 2 show that EGFR phosphorylation in AS and MEC is common phenomenon after OGD/R.

3.2 EGFR blockade ameliorate OGD/R-induced disruption of BSCB in vitro

Recent studies have demonstrated that EGFR signal path is involved in functional regulation of cell barrier, including BSCB[8, 14, 20]. In order to assess whether blocking EGFR signal pathway could ameliorate disruption of BSCB after OGD/R injury, FITC-Dextran extravasation and TEER measurements were performed to assess permeability BSCB mode *in vitro* with OGD/R damage in this study. Following OGD reoxygenation at 3 ~ 24 h, FITC-Dextran extravasation in the OGD/R group was significantly higher than in the control group at each experimental time point, which indicates that OGD/R leads to disruption of BSCB *in vitro*. However, a qualitative analysis showed EGFR inhibitor effectively mitigated FITC-Dextran extravasation in BSCB with OGD/R damage (Fig. 3A), implying that PD168393 inhibited BSCB disruption after OGD/R injury. The result of TEER measurements showed that OGD/R leads to TEER values of BSCB significantly decrease, while EGFR inhibitor prevented the negative effects of OGD/R on TEER values of BSCB (Fig. 3B). These results indicate that EGFR blockade ameliorates OGD/R-induced disruption of BSCB *in vitro*.

3.3 EGFR blockade inhibits NF-κB nuclear translocation and alleviates TJ protein loss and cytokine production in BSCB model in vitro following OGD/R.

To investigate the effects of EGFR/p38MAPK/NF-κb signaling pathway on expression of TJ proteins and pro-inflammatory factors, p38 expression, NF-κB nuclear translocation, TJ proteins expression, and pro-inflammatory factors levels were quantified. Using western blot and immunofluorescence, NF-κB nuclear translocation (Fig. 4A, B) and p38 upregulation (Fig. 4E, F) was significantly increased in the OGD/R group as compared with the control group. TJ protein (ZO-1 and occludin) expression in the OGD/R group was significantly less than the control group (Fig. 4C, D). Interestingly, EGFR inhibitor inhibited NF-κB nuclear translocation (Fig. 4A, B), p-p38 expression (Fig. 4E, F), and tight junction protein loss in a BSCB model after OGD/R damage (Fig. 4C,D. G1- H3). Using ELISA, the expression of TNF-α(Figure 4I), iNOS (Fig. 4J), COX-2 (Fig. 4K) and IL-1β (Fig. 4L) increased significantly in OGD/R group compare to control group. Importantly, EGFR blockade could not only inhibits EGFR/P38/NF-κB activation and alleviates TJ protein loss but also inhibit pro-inflammatory factors production (Fig. 4I-L) in BSCB model *in vitro* following OGD/R.

3.4 EGFR activation leads to p38 Activation, NF-κB nuclear translocation in primary astrocytes after OGD/R.

In order to assess the expression characteristics of EGFR downstream effector proteins in astrocytes after OGD/R, p38 and NF-κB protein levels were measured during EGFR activation with EGFR overexpression and EGFR inhibition with an inhibitor or EGFR shRNA. pEGFR, p-p38, p-NF-κB expression were significantly increased in the OGD/R group, Vehicle group, EGFR scramble shRNA group, CTL-EGFR

overexpression group, and the EGFR overexpression group (Fig. 5A, B). It is of note that EGFR overexpression increased downstream targets more than OGD/R treatment (in this figure as well as latter ones) and perhaps a lower concentration should be used in future experiments for a positive control. The levels of pEGFR, p-p38, and p-NF-κB protein were significantly reduced in the PD168393 and EGFR shRNA groups. Breifly, EGFR downstream effector proteins p-p38 and p-NF-κB increased following EGFR activation and decreased following EGFR inactivation.

To investigate EGFR activation influence on NF-κB nuclear translocation in primary astrocytes after OGD/R, immunofluorescent co-localization (p65 + DAPI) and Western blot was used to detect expression levels of NF-κB in the nucleus and cytoplasm. EGFR activation promotes NF-κB (p65) nuclear translocation in astrocytes with OGD/R damage, while EGFR inhibition ameliorates this translocation (Fig. 5C1-G).

3.5 p38 activation leads to NF-κB nuclear translocation in primary astrocytes after OGD/R.

NF-κB, a downstream target of p38, was analyzed in astrocytes after OGD/R, during activation of p38 by an agonist or inhibition by an inhibitor or p38 shRNA. p-p38 and p-NF-κB protein levels were significantly increased in the OGD/R group, Vehicle group, p38 scramble shRNA group, Ctrl-p38 overexpression group, and the p38 overexpression group (Fig. 6A, B). p-p38 and p-NF-κB levels were significantly reduced in the SB203580 (a p38 inhibitor) group and p38 shRNA group. This shows that p38 downstream signal molecular protein p-NF-κB increased following p38 activation and decreased following p38 inactivation.

To investigate p38 activation influence on NF-κB nuclear translocation in primary astrocytes after OGD/R, immunofluorescence (p65 + DAPI) and Western blot were used to detect protein levels of NF-κB (p65) in the nucleus and cytoplasm. p38 activation promotes NF-κB (p65) nuclear translocation in astrocytes with OGD/R damage, while p38 inactivation inhibited NF-κB nuclear translocation (Fig. 6C1-G).

3.6 EGFR activation leads to p38 Activation, NF-κB nuclear translocation in primary MEC after OGD/R.

EGFR downstream effector protein levels in MEC after OGD/R, p38 and NF-κB during EGFR activation by overexpression and inactivation by EGFR inhibitor or EGFR shRNA were analyzed. The levels of p-EGFR, p-p38, and p-NF-κB expression were significantly increased in the OGD/R group, Vehicle group, EGFR scramble shRNA group, CTL-EGFR overexpression group, and EGFR overexpression groups and significantly decreased in the PD168393 group and EGFR shRNA groups (Fig. 7A, B). Hence, EGFR downstream effector proteins (p-p38, p-NF-κB) increase following EGFR activation and decrease following EGFR inactivation in primary MEC after OGD/R.

To investigate EGFR activation influence on NF-κB nuclear translocation in primary MEC after OGD/R, immunofluorescence (p65 + DAPI) and Western blot were employed. EGFR activation promotes NF-κB (p65) nuclear translocation in primary MEC after OGD/R, while its inhibition diminishes NF-κB (p65) nuclear translocation (Fig. 7C1-G).

3.7 p38 activation leads to NF-κB nuclear translocation in primary MEC after OGD/R.

Targets of p38 in primary MEC after OGD/R, NF-κB were analyzed during p38 activation with a p38 agonist and p38 inactivation with a p38 inhibitor or p38 shRNA. p-p38, and p-NF-κB expression were significantly increased in the OGD/R group, Vehicle group, p38 scramble shRNA group, Ctrl-p38 overexpression group, and p38 overexpression groups and significantly decreased in the SB203580 and p38 shRNA groups. (Fig. 8A, B). Overall, p38 downstream target p-NF-κB increased following p38 activation and decreased following p38 inactivation.

To investigate the role p38 activation plays in NF-κB nuclear translocation in primary MEC after OGD/R, immunofluorescence co-localization (p65 + DAPI) and Western blot were used. p38 activation promotes NF-κB (p65) nuclear translocation in primary MEC after OGD/R, while p38 inactivation inhibited NF-κB (p65) nuclear translocation (Fig. 8C1**-G**).

3.8 EGFR inhibitor suppresses excessive EGFR activation in AS and MEC and excessive astrogliosis following SCI.

To examine whether EGFR activation in AS and MEC was a common phenomenon following SCI and ascertain whether early treatment of EGFR inhibitor PD168393 can inhibit EGFR activation in AS and MEC *in vivo*, double-immunofluorescent labeling for pEGFR and GFAP at one week after SCI was performed. As shown in Fig. 9, there was nearly no co-localization of pEGFR and GFAP in the intact spinal cord, indicating that quiescent astrocytes do not exist with EGFR phosphorylation (Fig. 9A1). However, in the injured spinal cord, most of astrocytes showed increased pEGFR immunoreactivity surrounding the lesion center (Fig. 9A3). These results are agreement with our previous studies[17, 19]. Furthermore, co-localization of pEGFR and CD31 in the intact spinal cord hardly existed (Fig. 9B1), while co-localization of pEGFR and CD31 occurred in a large number of MEC in the injured group (Fig. 9B3). More importantly, PD168393 administration effectively inhibited pEGFR immunoreactivity in both AS and MEC (Fig. 9A2 and B2) and inhibited excessive astrogliosis (Fig. 9C and D). These results show that EGFR phosphorylation is the main event of BSCB disruption (in AS and MEC) after SCI and was a common to all conditions in which injury was produced.

3.9 EGFR inhibitor attenuates BSCB disruption after SCI

EGFR activation may have a close relationship with BSCB disruption as EGFR phosphorylation of BSCB following SCI is a common phenomenon. In order to investigate whether EGFR activation could play a key role in BSCB damage and secondary injury after SCI and determine whether EGFR inhibitor treatment could ameliorate BSCB damage, Evans blue dye extravasation and water content of spinal cord were performed to measure BSCB permeability and spinal cord edema. As shown in the Fig. 10, very little Evans blue dye was found to leak into the spinal cord of control group (Fig. 10A1). A large amount of Evans blue dye extravasation at the lesion in spinal cord of injury group (Fig. 10A2). Evans blue dye extravasation around the lesion in the spinal cord of treatment group was significantly less than the injury group (Fig. 10A3, B). Similar results were shown in Evans blue fluorescence images of spinal cord transverse section (Fig. 10C1-C3, D), which indicated that EGFR inhibitor reduces Evans blue dye extravasation at the lesion after SCI. The measurement of the spinal cord water content showed that

water content in the injured group was the largest and EGFR inhibitor reduced water content in the treatment group (Fig. 10E). Together, these results suggest that the EGFR inhibitor attenuates BSCB disruption after SCI.

3.10 EGFR blockade suppresses EGFR-p38MAPK/NF-κB activation and alleviates TJ protein loss and pro-inflammatory cytokine production after SCI

Continual infusion of EGFR inhibitor (PD168393) was performed on rats immediately after SCI. EGFR activation after SCI results in the activation of p38MAPK cascades and potentially in modulating TJ proteins and pro-inflammatory factors. We first investigated whether EGFR downstream signal molecule was activated following SCI and if an EGFR inhibitor could influence EGFR downstream signal molecule expression. EGFR downstream signal molecule p38 and NF-κB present massive activate after SCI. And PD168393 (EGFR inhibitor) inhibited not only EGFR activation but also p38 and NF-κB activation at different timepoints (3d,7d and 14d after SCI)(Fig. 11A-D).

Following SCI, EGFR activation in BSCB could potentially modulate TJ proteins expression, we then determined whether EGFR inhibitor would directly influence expression of ZO-1 and occludin after SCI. Spinal cord sections were immunostained for co-localization of CD31 and ZO-1 or occludin at 3 days after SCI. Double staining of ZO-1 (or occludin) and CD31 revealed that TJ protein loss was most obvious in the injury group and EGFR blockade (PD168393) inhibited TJ protein loss after SCI (Fig. 11E1-F3). Western blot results also supported that EGFR blockade could alleviates TJ protein loss after SCI (Fig. 11G-H).

Further evaluation of whether the EGFR inhibitor could influence pro-inflammatory factor expression was tested. Using RT-PCR, it was found that activation of EGFR after SCI resulted in signficant upregulation of mRNA level of pro-inflammatory factors TNF-α, iNOS, COX-2, and IL-1β. EGFR inhibitor effectively reduced these pro-inflammatory factor mRNA levels (Fig. 11I-J). The results showed upregulation of pro-inflammatory factors TNF-α, iNOS, COX-2, and IL-1β after SCI was also significantly suppressed by EGFR blockade. Western blot results also supported that inhibition EGFR activation alleviated upregulation of pro-inflammatory factors after SCI (Fig. 11K-L).

Discussion

The present study shows the expression of EGFR was significantly increased in AS and MEC after SCI. Moreover, the EGFR-p38/NF-κB signaling pathways were also activated in AS and MEC after SCI. Further, activation of EGFR and its downstream p38 MAPK/NF-κB signaling could potentiate expression of pro-inflammatory factor and reduce expression of TJ protein after SCI, which lead to destruction of BSCB and secondary injury following SCI. These effects were attenuated by inhibition of EGFR in a rat model with SCI *in vivo* and a BSCB damage model *in vitro*. Together these results suggest that EGFR activating plays a key role in the pathobiology of BSCB damage and secondary injury following SCI.

BSCB is mainly formed by non-fenestrated capillary endothelial cells, a basal lamina, pericytes, astrocyte foot processes, and tight junctions[30]. The BSCB, a highly restrictive and permeable membrane structure dedicated to maintaining the steady state of spinal cord microenvironment, is a specialized interface between peripheral blood systems and the central nervous system (spinal cord)[31, 32]. Damage to the vasculature and breakdown of the BSCB is a universal consequence of SCI, clinically as well as in animal models[33]. The BSCB disruption plays an important role in the pathophysiology of secondary damage following SCI[8, 30]. The tight junction proteins (occludin, claudin-5, and ZO-1) are rapidly degraded at 8 h to 1 day following SCI and the permeability of BSCB in damage zone rapidly increased[33, 34], which triggers several factors involved in the pathophysiology of SCI, including edema, hemorrhaging, oxidative stress, and free radicals, as well as inflammatory damage[8, 35]. Therefore, protecting the structural and functional integrity of BSCB is the essential strategic measure to eliminate secondary damage and reconstruct the normal state of neural tissue microenvironment after SCI[8, 35].

EGFR is a receptor tyrosine-protein kinase (TPK) in the plasma membranes, which plays a crucial regulatory role in cell survival, growth, differentiation, proliferation, apoptosis, and other signal pathways[36]. Recently, increasing evidence has suggested that EGFR has also been shown to participate in microvascular injury in diabetes, intestinal permeability, and BSCB permeability after SCI[12, 13], indicating a role for EGFR in cellular barrier function[20]. Previous studies have demonstrated that EGFR activation was significant not only in astrocytes but also in microglia after SCI[17, 19, 28, 37]. Moreover, it was observed that EGFR in microvascular endothelial cells were similarly activated following SCI. As well-known, microvascular endothelial cells and astrocytes are the main component cells of BSCB. TJ protein loss, a notably increase in inflammatory factors, and continued destruction of BSCB was observed in response to EGFR activation in main component cells of BSCB both *in vivo* and *in vitro*. At the same time, inhibiting EGFR activation after SCI alleviated the disruption of BSCB, which implies that excessive EGFR activation in AS and MEC is responsible for damage to the BSCB.

Several studies have confirmed local application of EGFR inhibitor in SCI rats significantly improved locomotor, sensory, and bladder recovery after SCI in rats[17, 19, 37, 38]. Our previous studies have demonstrated that EGFR inhibitor PD168393 ameliorated excessive reactive astrogliosis and inhibited the production of inflammatory factors, and eventually facilitating a more favorable environment for axonal regeneration after SCI[17, 19]. The present study further revealed that the main component cells of the BSCB (MEC and AS) showed a large amount of EGFR activation after SCI. Inhibition of EGFR activation can significantly reduce damage of BSCB after SCI, thereby improve the neurological function deficit symptoms [18, 19, 26, 36]. Therefore, EGFR activation plays a key role in BSCB destruction and secondary spinal cord injury after SCI[18].

These studies confirmed that EGFR inhibition significantly reduced the loss of tight junction protein and the expression of inflammatory factors both after SCI and OGD/R damage of BSCB *in vitro*. The abnormal expression of inflammatory factors and tight junction proteins is directly related to the destruction of the BSCB[8]. EGFR, its downstream signal molecular p38, and NF-κB signaling pathways were also activated in a time dependent manner in a rat model with SCI and OGD/R damage of BSCB *in*

vitro. EGFR shRNA or EGFR inhibitor markedly attenuated BSCB permeability and production of pro-inflammatory factor, and activation of the EGFR/p38/NF-κB pathway both in vivo and *in vitro*. Moreover, inhibiting EGFR activation could significantly reduce nuclear translocation of NF-κB, which regulates the expression of genes such as tight junction protein and pro-inflammatory cytokines, leading to the loss of the tight junction protein and inflammation damage after SCI. These results demonstrate the important role of the EGFR/p38/NF-κB signaling pathway in regulating the expression of tight junction proteins and pro-inflammatory cytokines after SCI. A Schematic model has been made showing the possible interaction between EGFR and p38/NF-κB pathway (Fig. 12).

Conclusions

In conclusion, it has been shown that activation of EGFR and its downstream p38MAPK/NF-κB signaling pathway in AS and MEC contributes to the regulation of BSCB TJ integrity, thereby shedding light on the mechanistic pathway that links the pathology of secondary injury after SCI. These findings not only provide evidence for a potential mechanism in the pathogenesis of BSCB disruption and secondary injury in SCI, but also provide a potential target for therapeutic measures to achieve effective control of the development and progression of BSCB and secondary injury in SCI.

Abbreviations

EGFR epidermal growth factor receptor, BSCB blood spinal cord barrier, AS astrocytes, SCI spinal cord injury, MEC microvascular endothelial cells, OGD/R oxygen and glucose deprivation/reoxygenation, MAPK mitogen-activated proteins kinase, shRNA short hairpin Ribonucleic Acid, TNF-α tumor necrosis factor α, iNOS inducible Nitric Oxide Synthase, COX-2 cyclooxygenase-2, IL-1β Interleukin-1β, TJ tight junction, TEER transendothelial electrical resistance, FITC fluorescein isothiocyanate, NF-κB nuclear factor-kappa B, SCMEC spinal cord microvascular endothelial cells, ip intraperitoneal, PBS phosphate buffer saline, DMEM dulbecco's modified eagle medium, FBS fatal bovine serum, DMSO dimethyl sulfoxide, GFAP glial fibrillary acidic protein, CD31 cell adhesion molecule-1, HBSS Hanks' Balanced Salt Solution, pEGFR phosphorylated epidermal growth factor receptor, DAPI 4',6-diamidino-2-phenylindole, BSA bovine serum albumin, ECL enhanced chemiluminescence, OD optical density, GAPDH glyceraldehyde-3-phosphate dehydrogenase, ERS-2 european remote sensing satellite 2, SD standard deviation, ANOVA one-way analysis of variance, TPK tyrosine-protein kinase

Declarations

Acknowledgements

We thank Clarity Manuscript Consultants for manuscript editing.

Funding

This work was supported by a Natural Science Foundation of China (NFSC) grant (81671219, 82071364, 81760881, 81901259), Natural Science Foundation of Jiangsu Province (BK20180168)Medical Young Talents Program of Jiangsu Province (QNRC2016191), Shenzhen Special Fund for Basic Research (Shenzhen Natural Science Foundation, JCYJ20190806145812589), and Double-Hundred Medical Talents Program of Wuxi City (HB2020016, HB2020015).

Availability of data and materials

Not applicable.

Authors' contributions

ZWL, YG and GJX participated in the design of the research. ZWL, JJZ, SYL, CTT, YW and QW carried out the experiments, acquired and analyzed the data. YG, ZWL and GJX provided technical support during the experiments. GJX supervised the study. ZWL, YG and GJX wrote and revised the manuscript. All authors read and approved the final manuscript.

Competing interests

The authors declare that they have no competing interests.

Consent for publication

Not applicable.

Ethics approval and consent to participate

Animal procedures were performed in strict accordance with protocols approved by the Institutional Animal Care and Use Committee at Jinan University with the number #10453.

References

1. Manley NC, Priest CA, Denham J, Wirth ED, 3rd, Lebkowski JS: **Human Embryonic Stem Cell-Derived Oligodendrocyte Progenitor Cells: Preclinical Efficacy and Safety in Cervical Spinal Cord Injury**[J]. *Stem Cells Transl Med* 2017,**6**:1917-1929.
2. Bolouri H, Zetterberg H. Animal Models for Concussion: Molecular and Cognitive Assessments-Relevance to Sport and Military Concussions. In: Kobeissy FH, editor. Brain Neurotrauma: Molecular, Neuropsychological, and Rehabilitation Aspects. Frontiers in Neuroengineering. Boca Raton (FL)2015.
3. Tran AP, Warren PM, Silver J: **The Biology of Regeneration Failure and Success After Spinal Cord Injury**[J]. *Physiol Rev* 2018,**98**:881-917.
4. Zhang D, Wang Q, Wang S, Huang Y, Tian N, Wu Y, Wu Y, Zhou Y, Xu H, Zhang X: **Astragoloside IV Loaded Polycaprolactone Membrane Repairs Blood Spinal Cord Barrier and Recovers Spinal Cord**

Function in Traumatic Spinal Cord Injury[J]. *J Biomed Nanotechnol* 2019,**15**:799-812.

5. Xue W, Tan W, Dong L, Tang Q, Yang F, Shi X, Jiang D, Qian Y: **TNFAIP8 influences the motor function in mice after spinal cord injury (SCI) through meditating inflammation dependent on AKT**[J]. *Biochem Biophys Res Commun* 2020,**528**:234-241.
6. Jiang D, Gong F, Ge X, Lv C, Huang C, Feng S, Zhou Z, Rong Y, Wang J, Ji C, Chen J, Zhao W, Fan J, Liu W, Cai W: **Neuron-derived exosomes-transmitted miR-124-3p protect traumatically injured spinal cord by suppressing the activation of neurotoxic microglia and astrocytes**[J]. *J Nanobiotechnology* 2020,**18**:105.
7. Gensel JC, Zhang B: **Macrophage activation and its role in repair and pathology after spinal cord injury**[J]. *Brain Res* 2015,**1619**:1-11.
8. Cai XJ, Zhao JJ, Lu Y, Zhang JP, Ren BY, Cao TT, Xi GJ, Li ZW: **The microenvironment following oxygen glucose deprivation/re-oxygenation-induced BSCB damage in vitro**[J]. *Brain Res Bull* 2018,**143**:171-180.
9. Haggerty AE, Maldonado-Lasuncion I, Oudega M: **Biomaterials for revascularization and immunomodulation after spinal cord injury**[J]. *Biomed Mater* 2018,**13**:044105.
10. Li XQ, Cao XZ, Wang J, Fang B, Tan WF, Ma H: **Sevoflurane preconditioning ameliorates neuronal deficits by inhibiting microglial MMP-9 expression after spinal cord ischemia/reperfusion in rats**[J]. *Mol Brain* 2014,**7**:69.
11. Wang C, Xu K, Wang Y, Mao Y, Huang Y, Liang Y, Liu Y, Hao J, Gu X, Ma Z, Sun Y: **Spinal cannabinoid receptor 2 activation reduces hypersensitivity associated with bone cancer pain and improves the integrity of the blood-spinal cord barrier**[J]. *Reg Anesth Pain Med* 2020,**45**:783-791.
12. Chen F, Hori T, Ohashi N, Baine AM, Eckman CB, Nguyen JH: **Occludin is regulated by epidermal growth factor receptor activation in brain endothelial cells and brains of mice with acute liver failure**[J]. *Hepatology* 2011,**53**:1294-1305.
13. Tang X, Liu H, Yang S, Li Z, Zhong J, Fang R: **Epidermal Growth Factor and Intestinal Barrier Function**[J]. *Mediators Inflamm* 2016,**2016**:1927348.
14. Ogawa M, Kojima T, Someya M, Nomura K, Takasawa A, Murata M, Tanaka S, Saito T, Sawada N: **Epidermal growth factor modulates claudins and tight junctional functions in ovarian cancer cell lines**[J]. *Histochem Cell Biol* 2012,**138**:323-338.
15. Liu M, Solomon W, Cespedes JC, Wilson NO, Ford B, Stiles JK: **Neuregulin-1 attenuates experimental cerebral malaria (ECM) pathogenesis by regulating ErbB4/AKT/STAT3 signaling**[J]. *J Neuroinflammation* 2018,**15**:104.
16. Yang Q, Wang EY, Huang XJ, Qu WS, Zhang L, Xu JZ, Wang W, Tian DS: **Blocking epidermal growth factor receptor attenuates reactive astrogliosis through inhibiting cell cycle progression and protects against ischemic brain injury in rats**[J]. *J Neurochem* 2011,**119**:644-653.
17. Li ZW, Tang RH, Zhang JP, Tang ZP, Qu WS, Zhu WH, Li JJ, Xie MJ, Tian DS, Wang W: **Inhibiting epidermal growth factor receptor attenuates reactive astrogliosis and improves functional outcome after spinal cord injury in rats**[J]. *Neurochem Int* 2011,**58**:812-819.

18. Yan P, Wu X, Liu X, Cai Y, Shao C, Zhu G: **A Causal Relationship in Spinal Cord Injury Rat Model Between Microglia Activation and EGFR/MAPK Detected by Overexpression of MicroRNA-325-3p**[J]. *J Mol Neurosci* 2019,**68**:181-190.
19. Li ZW, Li JJ, Wang L, Zhang JP, Wu JJ, Mao XQ, Shi GF, Wang Q, Wang F, Zou J: **Epidermal growth factor receptor inhibitor ameliorates excessive astrogliosis and improves the regeneration microenvironment and functional recovery in adult rats following spinal cord injury**[J]. *J Neuroinflammation* 2014,**11**:71.
20. Kjell J, Pernold K, Olson L, Abrams MB: **Oral erlotinib, but not rapamycin, causes modest acceleration of bladder and hindlimb recovery from spinal cord injury in rats**[J]. *Spinal Cord* 2014,**52**:186-190.
21. Zhou Y, Zheng B, Ye L, Zhang H, Zhu S, Zheng X, Xia Q, He Z, Wang Q, Xiao J, Xu H: **Retinoic Acid Prevents Disruption of Blood-Spinal Cord Barrier by Inducing Autophagic Flux After Spinal Cord Injury**[J]. *Neurochem Res* 2016,**41**:813-825.
22. Shen Y, Sun A, Wang Y, Cha D, Wang H, Wang F, Feng L, Fang S, Shen Y: **Upregulation of mesencephalic astrocyte-derived neurotrophic factor in glial cells is associated with ischemia-induced glial activation**[J]. *J Neuroinflammation* 2012,**9**:254.
23. Codeluppi S, Gregory EN, Kjell J, Wigerblad G, Olson L, Svensson CI: **Influence of rat substrain and growth conditions on the characteristics of primary cultures of adult rat spinal cord astrocytes**[J]. *J Neurosci Methods* 2011,**197**:118-127.
24. Molino Y, Jabes F, Bonnet A, Gaudin N, Bernard A, Benech P, Khrestchatisky M: **Gene expression comparison reveals distinct basal expression of HOX members and differential TNF-induced response between brain- and spinal cord-derived microvascular endothelial cells**[J]. *J Neuroinflammation* 2016,**13**:290.
25. Hou QX, Yu L, Tian SQ, Jiang CJ, Yang WJ, Wang ZJ: **Neuroprotective effects of atomoxetine against traumatic spinal cord injury in rats**[J]. *Iran J Basic Med Sci* 2016,**19**:272-280.
26. Ye LB, Yu XC, Xia QH, Yang Y, Chen DQ, Wu F, Wei XJ, Zhang X, Zheng BB, Fu XB, Xu HZ, Li XK, Xiao J, Zhang HY: **Regulation of Caveolin-1 and Junction Proteins by bFGF Contributes to the Integrity of Blood-Spinal Cord Barrier and Functional Recovery**[J]. *Neurotherapeutics* 2016,**13**:844-858.
27. Kaptanoglu E, Okutan O, Akbiyik F, Solaroglu I, Kilinc A, Beskonakli E: **Correlation of injury severity and tissue Evans blue content, lipid peroxidation and clinical evaluation in acute spinal cord injury in rats**[J]. *J Clin Neurosci* 2004,**11**:879-885.
28. Qu WS, Tian DS, Guo ZB, Fang J, Zhang Q, Yu ZY, Xie MJ, Zhang HQ, Lu JG, Wang W: **Inhibition of EGFR/MAPK signaling reduces microglial inflammatory response and the associated secondary damage in rats after spinal cord injury**[J]. *J Neuroinflammation* 2012,**9**:178.
29. Hsu CY, Hogan EL, Gadsden RH, Sr., Spicer KM, Shi MP, Cox RD: **Vascular permeability in experimental spinal cord injury**[J]. *J Neurol Sci* 1985,**70**:275-282.
30. Reinhold AK, Rittner HL: **Barrier function in the peripheral and central nervous system-a review**[J]. *Pflugers Arch* 2017,**469**:123-134.

31. Sharma HS: **Early microvascular reactions and blood-spinal cord barrier disruption are instrumental in pathophysiology of spinal cord injury and repair: novel therapeutic strategies including nanowired drug delivery to enhance neuroprotection**[J]. *J Neural Transm (Vienna)* 2011,**118**:155-176.
32. Sharma HS: **Pathophysiology of blood-spinal cord barrier in traumatic injury and repair**[J]. *Curr Pharm Des* 2005,**11**:1353-1389.
33. Maikos JT, Shreiber DI: **Immediate damage to the blood-spinal cord barrier due to mechanical trauma**[J]. *J Neurotrauma* 2007,**24**:492-507.
34. Zhou Y, Wu Y, Liu Y, He Z, Zou S, Wang Q, Li J, Zheng Z, Chen J, Wu F, Gong F, Zhang H, Xu H, Xiao J: **The cross-talk between autophagy and endoplasmic reticulum stress in blood-spinal cord barrier disruption after spinal cord injury**[J]. *Oncotarget* 2017,**8**:1688-1702.
35. Shultz RB, Zhong Y: **Minocycline targets multiple secondary injury mechanisms in traumatic spinal cord injury**[J]. *Neural Regen Res* 2017,**12**:702-713.
36. Proto C, Imbimbo M, Gallucci R, Brissa A, Signorelli D, Vitali M, Macerelli M, Corrao G, Ganzinelli M, Greco FG, Garassino MC, Lo Russo G: **Epidermal growth factor receptor tyrosine kinase inhibitors for the treatment of central nervous system metastases from non-small cell lung cancer: the present and the future**[J]. *Transl Lung Cancer Res* 2016,**5**:563-578.
37. Erschbamer M, Pernold K, Olson L: **Inhibiting epidermal growth factor receptor improves structural, locomotor, sensory, and bladder recovery from experimental spinal cord injury**[J]. *J Neurosci* 2007,**27**:6428-6435.
38. Zhang S, Ju P, Tjandra E, Yeap Y, Owlanj H, Feng Z: **Inhibition of Epidermal Growth Factor Receptor Improves Myelination and Attenuates Tissue Damage of Spinal Cord Injury**[J]. *Cell Mol Neurobiol* 2016,**36**:1169-1178.

Figures

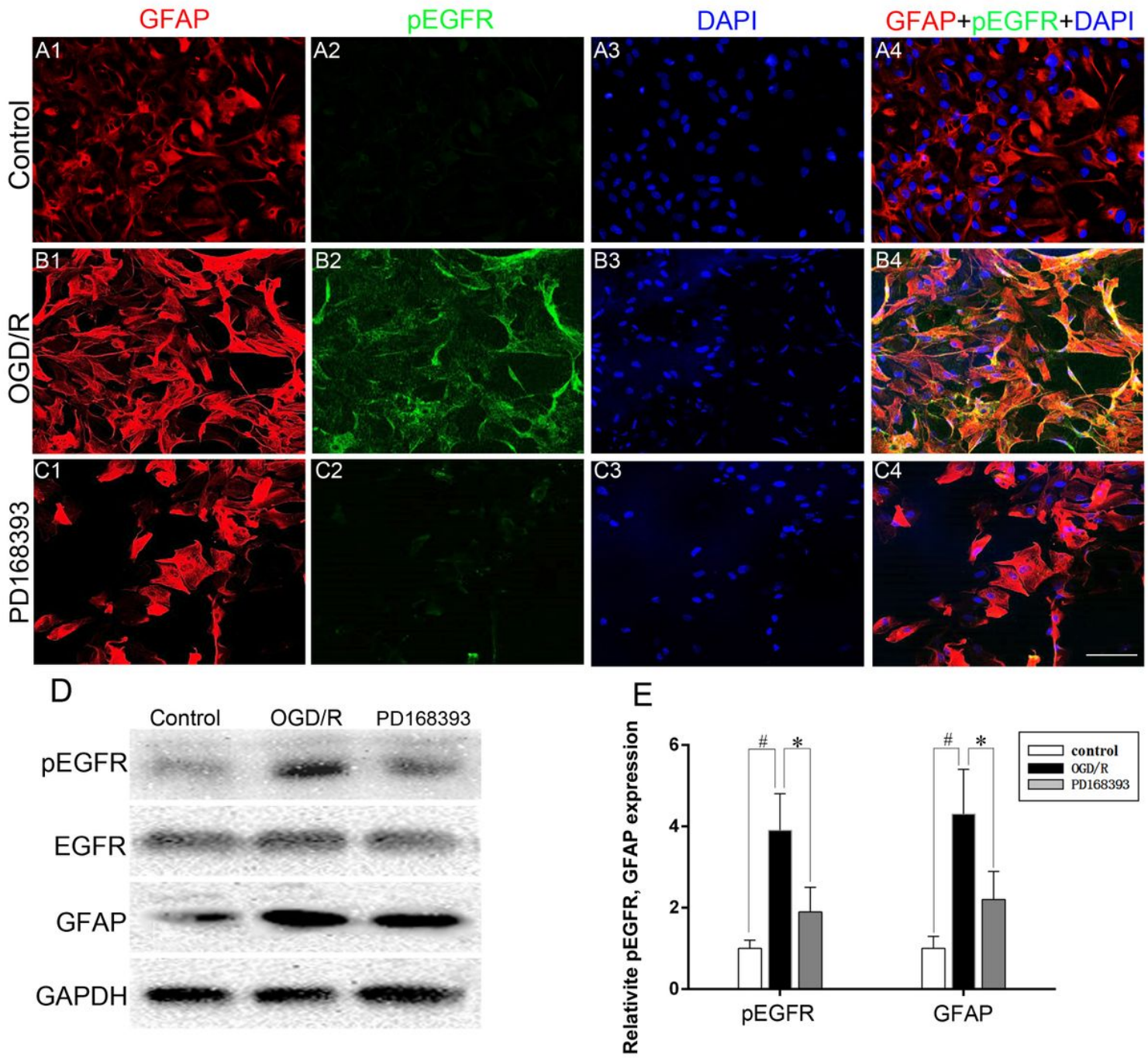

Figure 1

EGFR phosphorylation in astrocytes is elevated in parallel with astrogliosis in BSCB model in vitro following OGD/R. (A1-C4) Double staining of pEGFR and GFAP reveals that pEGFR+ reactive AS increase following OGD/R (B4) and lessen in the present of PD168393 (C4), but not in the control group(A4). Fluorescent staining of GFAP demonstrates activation of AS following OGD/R (B1-4). Bar = 50 μm. (D) Representative Western blots of pEGFR and GFAP expression are shown (n=3/group). (E) Semiquantitative analysis of pEGFR as a ratio of EGFR loading and semiquantitative measurements of GFAP were obtained by normalization to β-actin. *P□0.05, #P□0.01.

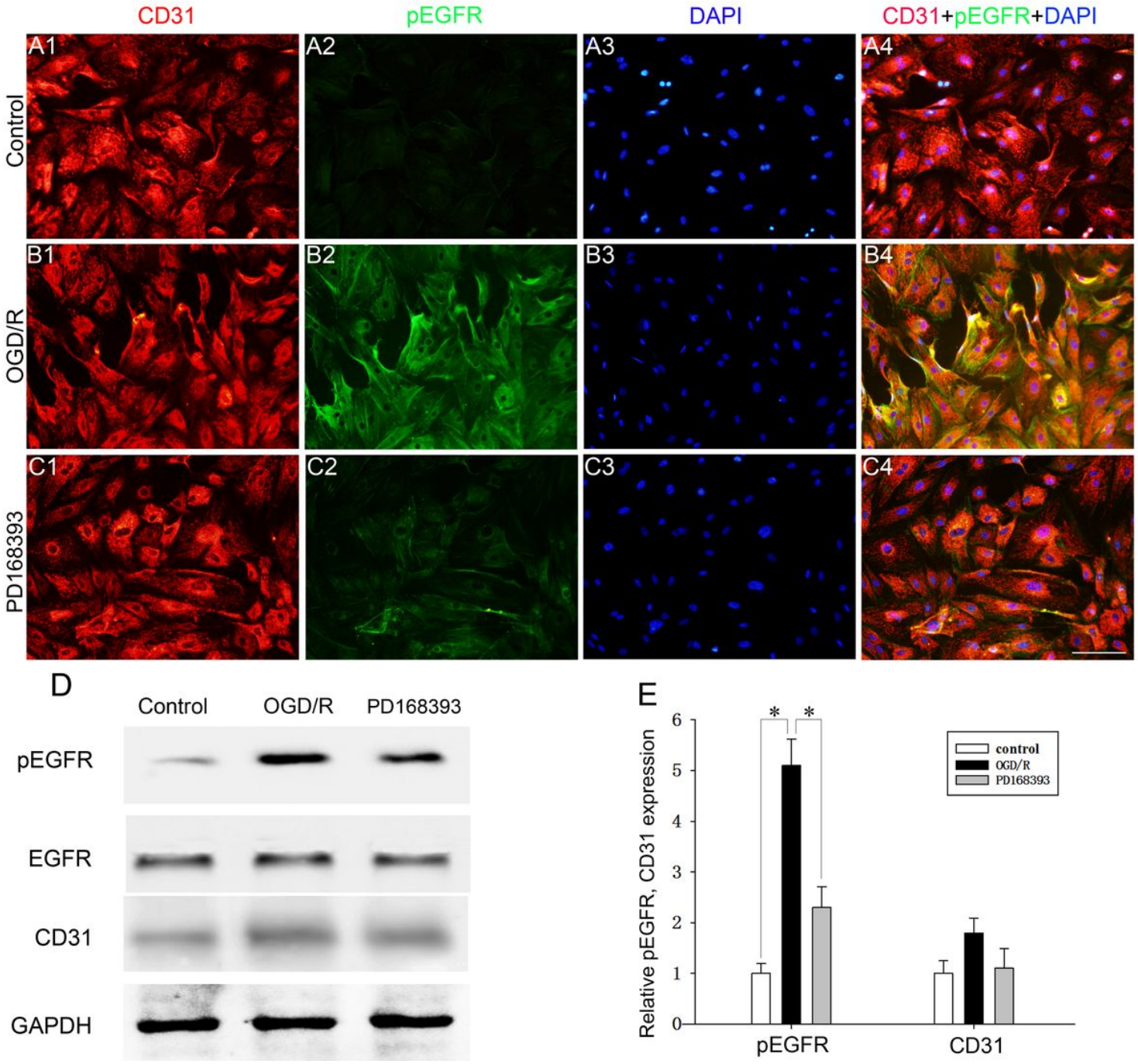

Figure 2

EGFR phosphorylation in MEC is elevated in BSCB model in vitro following OGD/R. (A1-C4) Double staining of pEGFR and CD31 reveals that pEGFR+ MEC increase obviously following OGD/R (B4) and lessen in the presence of PD168393 (C4), but not appear in the control group (A4). Bar=50 μm. (D) Representative Western blots of pEGFR and CD31 expression are shown (n=3/group). (E) Semiquantitative analysis of pEGFR as a ratio of EGFR loading and semiquantitative measurements of CD31 were obtained by normalization to GAPDH. *P□0.05.

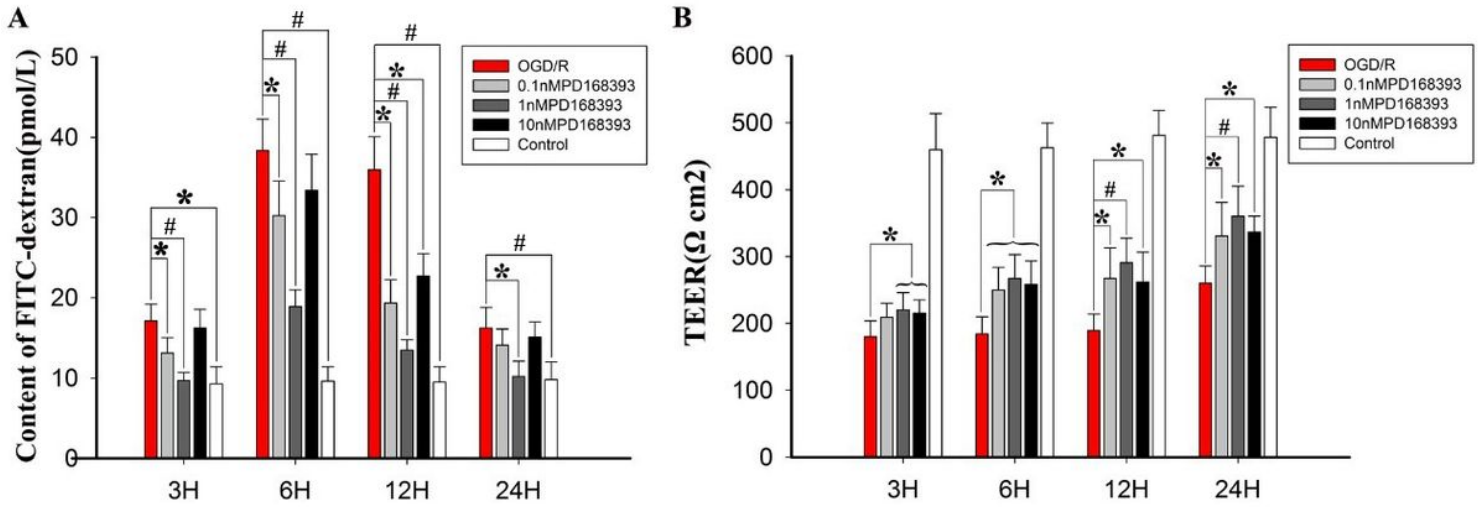

Figure 3

EGFR blockade attenuates permeability in a model of OGD/R damaged BSCB. (A) Bar graph shows the quantity of FITC-dextran leaking from the insert (upper chamber) into bottom chamber across MEC monolayers on Transwell culture system at different time points (3, 6, 12 and 24h after OGD/R) in different groups (treatment group includes 3 subgroups with different PD168393 concentration). * P < 0.05, # P <0.01. (B) Bar graph shows TEER values at different time intervals (3, 6, 12 and 24h after OGD/R) in different groups (treatment group includes 3 subgroups with different PD168393 concentrations) (n = 3/group) *P□0.05, #P□0.01.

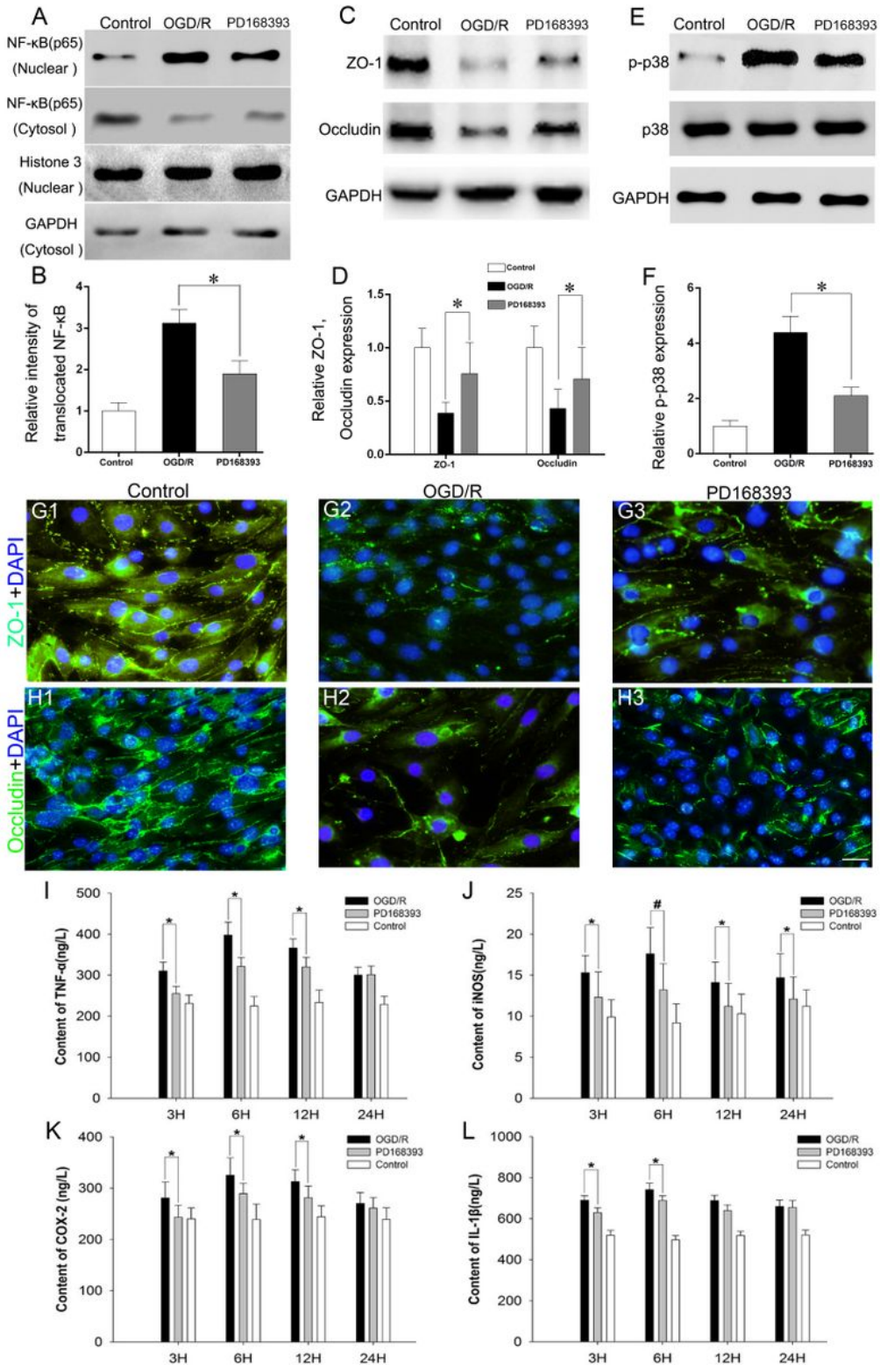

Figure 4

EGFR blockade inhibits NF-κB nuclear translocation, p-p38 expression and tight junction protein loss in a model of BSCB damage by OGD/R. (A) Representative Western blots of NF-κB in nucleus and cytoplasm expression (n = 3/group), Histone was a nuclear loading control and GAPDH was a cytosol loading control. (B) Semi-quantitative measurements of NF-κB were obtained by normalizing to Histone 3 in nucleus and GAPDH in cytoplasm respectively, *P < 0.05. (C) Representative Western blots of ZO-1 and

occludin expression (n = 3/group), GAPDH was the loading control. (D) Semi-quantitative measurements of ZO-1 and occludin were obtained by normalizing to GAPDH, * P < 0.05. (E) Representative Western blots of p-P38 and P38 expression (n = 3/group), and GAPDH was a loading control. (F) Semi-quantitative measurements of p-P38 and P38 were obtained by normalizing to GAPDH, * P < 0.05. (G1-G3) Cultured microvascular endothelial cells were immunostained for ZO-1 and DAPI in control (G1), injury, (G2) and PD168393 (1 nM) treatment groups (G3) at 24 hours after OGD/R (n = 5 in each group). (H1-H3) Cultured MEC were immunostained for occludin and DAPI in control (G1), OGD/R, (G2) and PD168393 (1 nM) treatment groups (G3) at 24 hours after OGD/R (n = 5 in each group). Scale bar=20μm in H3(applies to G1-H3). I-L Supernatants in three groups were collected respectively for ELISA to detect pro-inflammation factor expression. Effect of EGFR inhibitor PD168393 on the expression of TNF-α (I), iNOS(J), COX-2(K), and IL-1β(L) at different time points after BSCB with OGD/R damage in vitro. *P 0.05, #P 0.01.

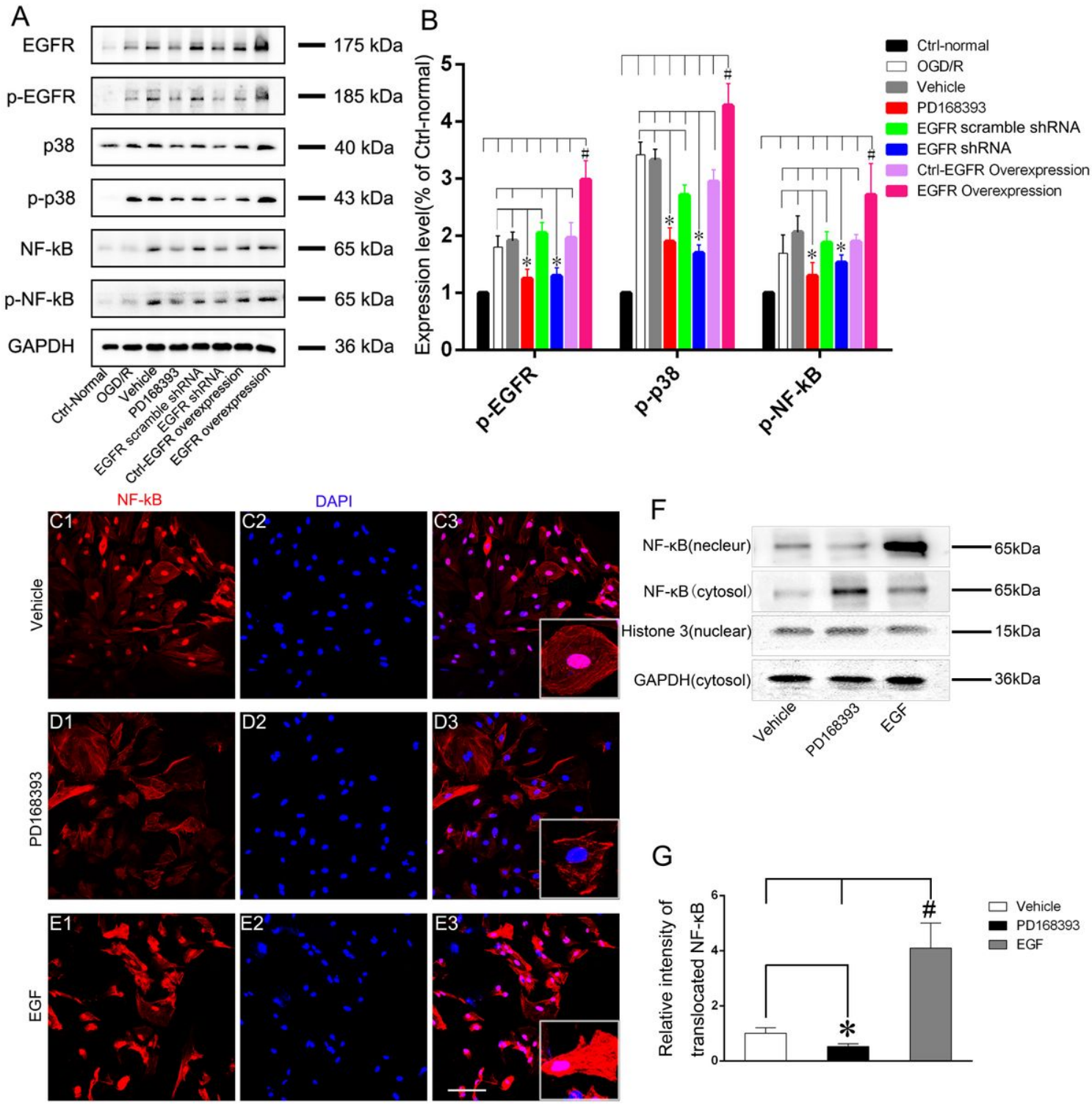

Figure 5

EGFR blockade decreases p38 Activation and NF-κB nuclear translocation in primary astrocytes after OGD/R. Primary spinal cord astrocytes were pretreated with the OGD/R procedure. EGFR downstream targets were then analyzed during activation and inhibition of EGFR via EGFR overexpression and EGFR inhibitor or EGFR shRNA, respectively. (A) Representative western blots of EGFR、pEGFR、p38、p-p38, NF-κB and p-NF-κB protein levels in different experimental treatment conditions (n = 3/group)、with GAPDH as a loading control. (B) Densitometric analysis of the pEGFR, p-p38, and p-NF-κB levels from blots. (C1-

E3) At 12 h of reoxygenation after OGD 3 h, the levels of NF-κB in the nucleus and cytoplasm were detected by immunofluorescence to determine the differences of NF- κB nuclear translocation (C1-C3), PD168393 (D1-D3) and EGF group (E1-E3). Insets in (C3), (D3) and (E3) are images shown in high magnification. Scale bar = 20 μm (applies to D1-E3). (F) Representative Western blot of NF-κB in nucleus and cytoplasm expression (n = 3/group), Histone was the nuclear loading control and GAPDH was the cytosol loading control. (G) Densitometric analysis of NF-κB (p65) nuclear translocation, *P□0.05, #P□ 0.01.

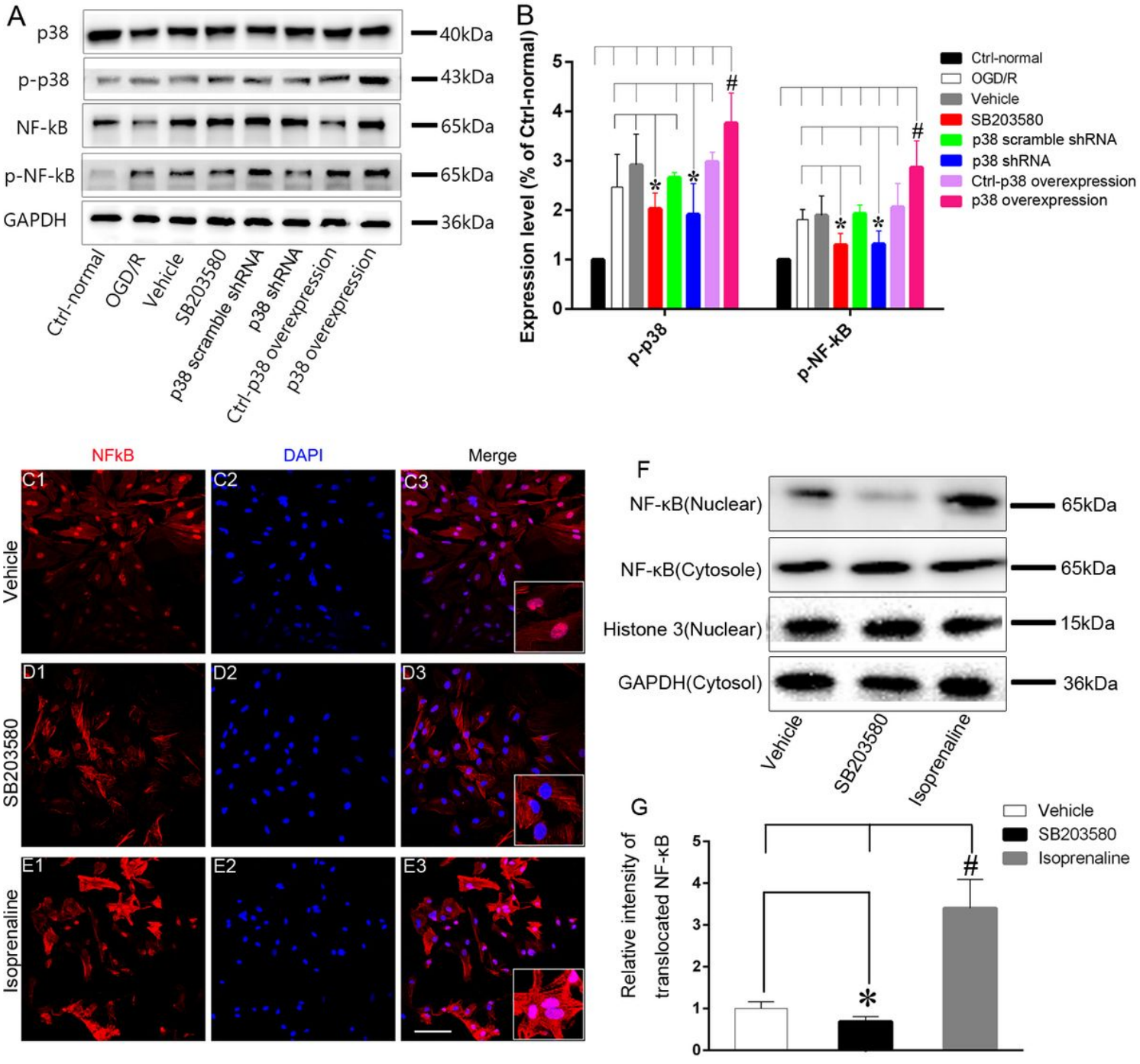

Figure 6

EGFR downstream p38 blockade lessens NF-κB nuclear translocation in primary astrocytes after OGD/R. Primary spinal cord astrocytes were pretreated with the OGD/R procedure. The expression characteristics of EGFR downstream effector proteins in astrocytes were analyzed under circumstance of p38 activation by p38 overexpression and p38 inactivation by p38 inhibitor or p38 shRNA. (A) Representative Western blots of p38, p-p38, NF-Kb, and p-NF-κB expression in different experimental treatment conditions (n = 3/group)． GAPDH as a loading control. (B) Densitometric analysis of p-p38 and p-NF-κB expression, *P＜ 0.05，#P＜0.01. (C1-E3) Immunoflourescent expression levels of NF-κB (p65) in the nucleus and cytoplasm at 12h of reoxygenation after OGD were detected by immunofluorescence and Western blot to determine the differences of NF- κB nuclear translocation in vehicle group (C1-C3), SB203580 (D1-D3) and Isoprenaline (p38 agonist) group (E1-E3). Insets in (C3), (D3), and (E3) are images shown in high magnification. Scale bar= 20 μm (applies to D1-E3). (F) Representative Western blots of NF-κB in nucleus and cytoplasm expression (n = 3/group), Histone was the nuclear loading control and GAPDH was the cytosol loading control. (G) Densitometric analysis of NF-κB (p65) nuclear translocation, *P＜0.05, #P＜ 0.01.

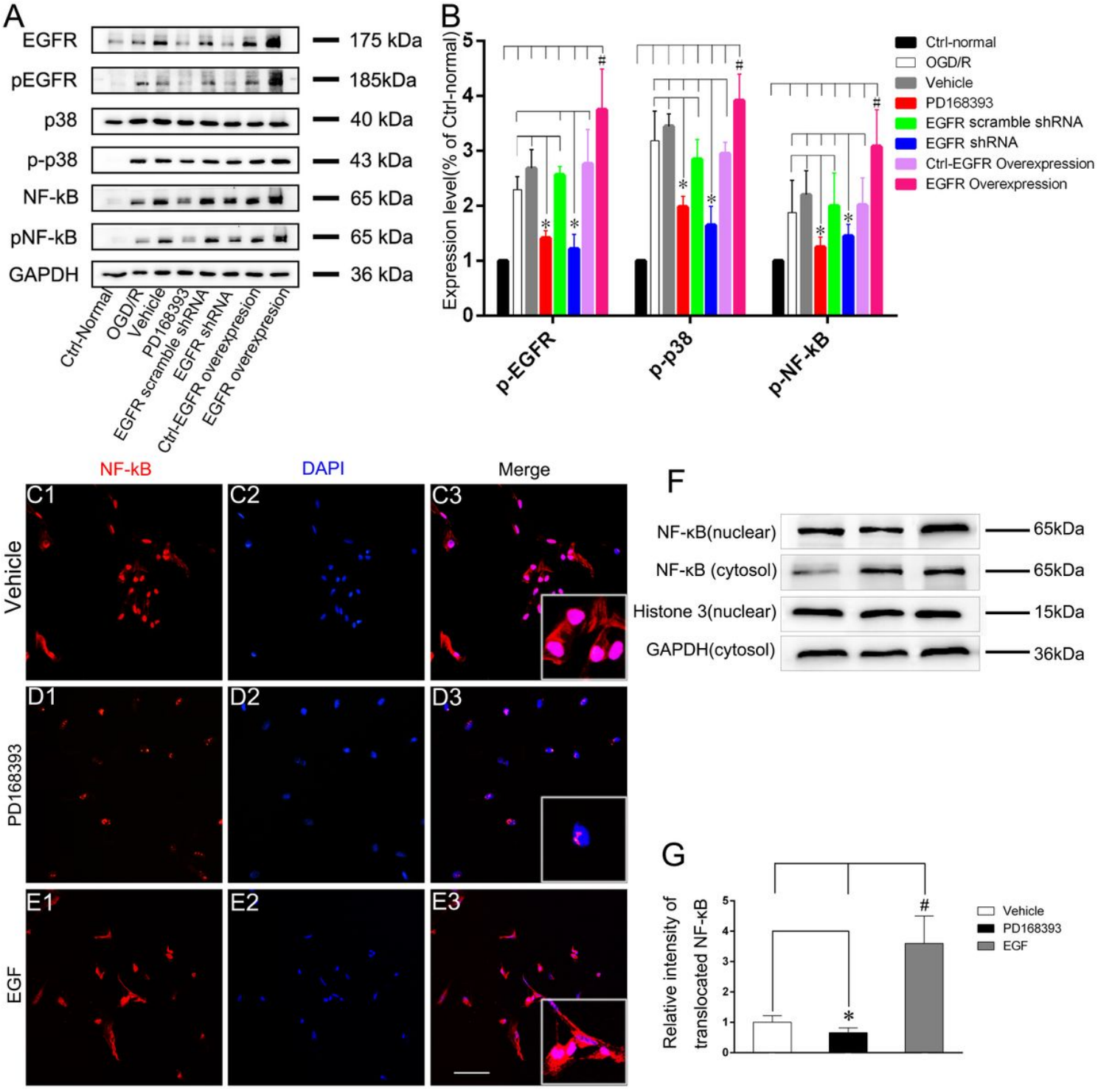

Figure 7

EGFR blockade decreases p38 Activation and NF-κB nuclear translocation in primary MEC after OGD/R. Primary spinal cord MEC were pretreated with the OGD/R procedure. Expression characteristics of EGFR downstream signal molecular protein in astrocytes were analyzed under circumstances of EGFR activation by EGFR overexpression and EGFR inactivation by EGFR inhibitor or EGFR shRNA. (A) Representative Western blots of EGFR、pEGFR、p38、p-p38、NF-κB and p-NF-κB protein levels in different experimental treatment conditions (n = 3/group)、with GAPDH as a loading control. (B) Densitometric

analysis of pEGFR, p-p38, and p-NF-κB protein levels. (C1-E3) At 12h of reoxygenation after OGD 3 h, immunofluorescence of NF- κB nuclear translocation in vehicle group (C1-C3), PD168393 (D1-D3) and EGF group (E1-E3). Insets in (C3), (D3), and (E3) are images shown in high magnification. Scale bar = 20 μm (applies to D1-E3). (F) Representative Western blots of NF-κB expression in nucleus and cytoplasm (n = 3/group), Histone was the nuclear loading control and GAPDH was the cytosol loading control. (G) Densitometric analysis of NF-Kb (p65) nuclear translocation, *P□0.05, #P□0.01.

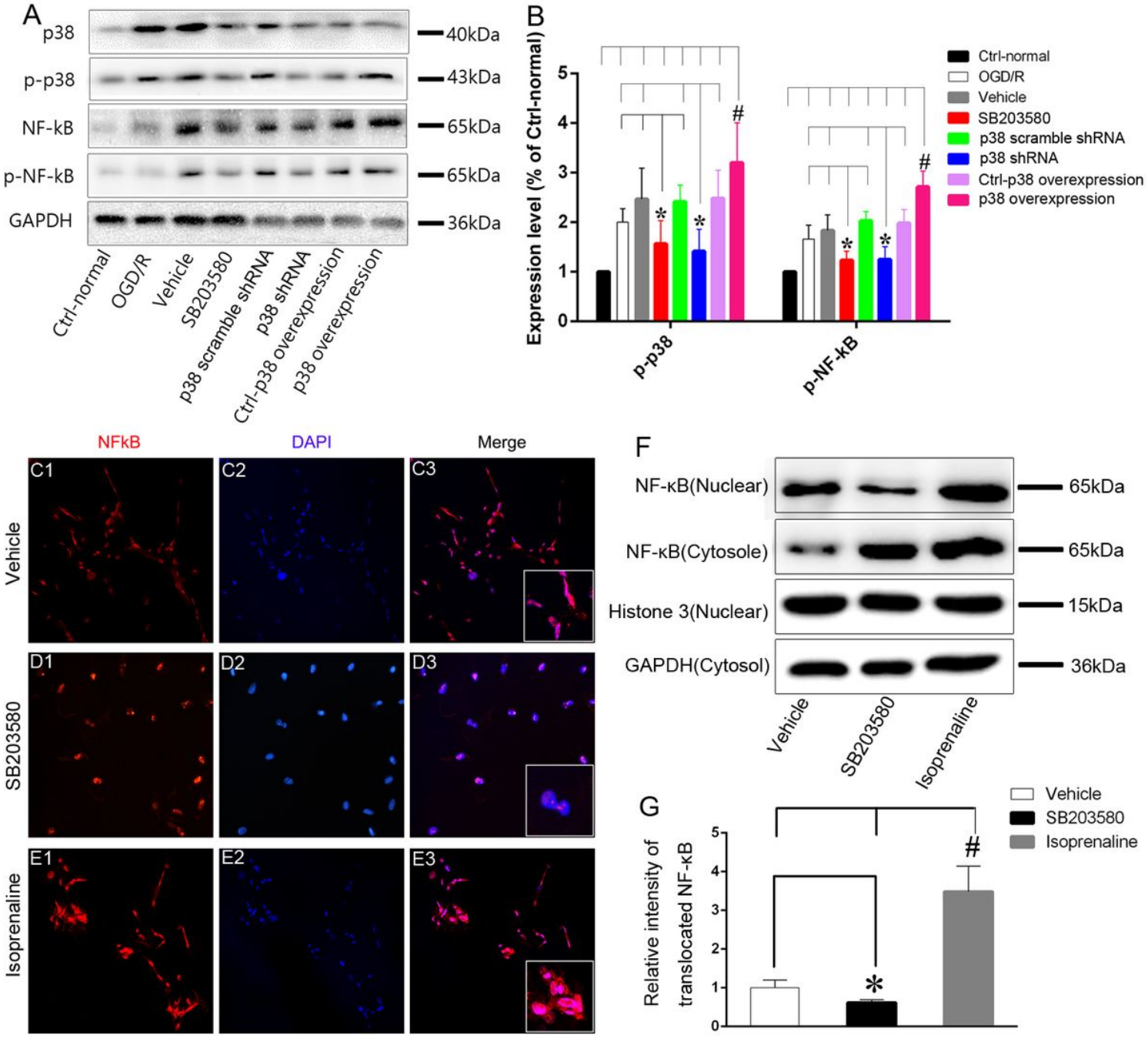

Figure 8

EGFR downstream p38 blockade lessens NF-κB nuclear translocation in primary MEC after OGD/R. Primary spinal cord MEC were pretreated with the OGD/R procedure. The expression characteristics of EGFR downstream effector proteins in astrocytes were analyzed under circumstance of p38 activation by

p38 overexpression and p38 inactivation by p38 inhibitor or p38 shRNA. (A) Representative western blots of p38、p-p38、NF-κB and p-NF-κB expression in different experimental treatment condition (n = 3/group)、with GAPDH as a loading control. (B) Densitometric analysis of p-p38, and p-NF-κB expression, *P＜0.05、#P＜0.01. (C1-E3) At 12h of reoxygenation after OGD 3 h, the expression levels of NF- B (NF- B) in the nucleus and cytoplasm were detected by Immunofluorescence and Western blot to determine the differences of NF- κB nuclear translocation in vehicle group(C1-C3), SB203580 (D1-D3) and Isoprenaline(p38 agonist) group(E1-E3). Insets in (C3), (D3) and (E3) are images shown in high magnification. Scale bar = 20 μm (applies to D1-E3). (F) Representative Western blots of NF-κB in the nucleus and cytoplasm (n = 3/group), Histone was the nuclear loading control and GAPDH was the cytosolic loading control. (G) Densitometric analysis of NF-κB (p65) nuclear translocation, *P＜0.05, #P＜0.01.

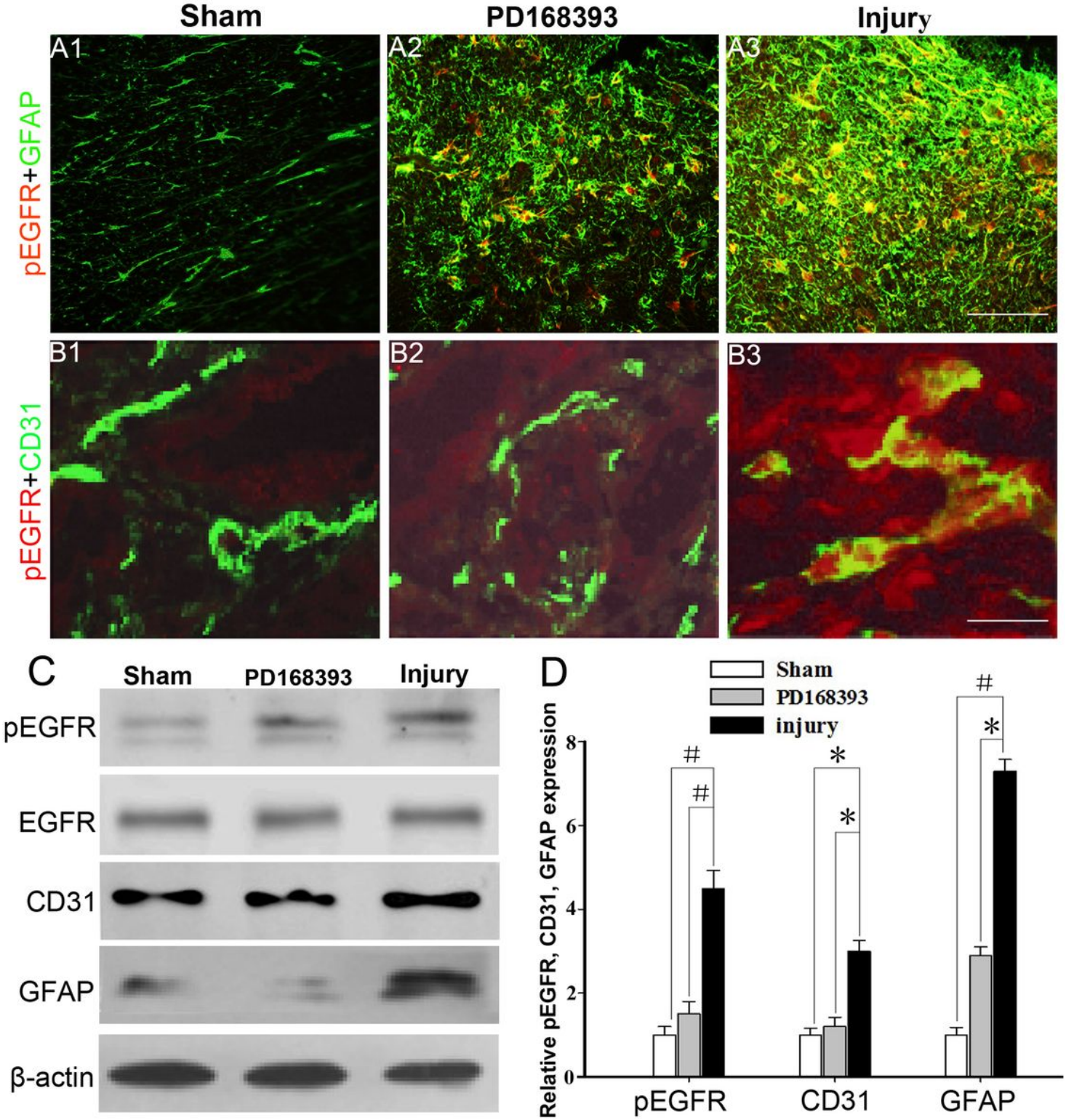

Figure 9

EGFR activation in AS and spinal cord MEC is significant after SCI and reduced by PD168393 (EGFR inhibitor), thereby suppressing excessive astrogliosis. (A1-A3) Spinal cord sections were immunostained for co-localization of pEGFR and glial fibrillary acid protein (GFAP) at one week after SCI (n = 5/group). Scale bars = 50 μm in A3(applies to A1-A3). (B1-B3) Spinal cord sections were immunostained for co-localization of pEGFR and CD31 (microvascular endothelial cell marker) at one week after SCI (n =

5/group). Scale bars = 10 μm in B3 (applies to B1-B3). (C) Representative Western blots of pEGFR, EGFR, CD31, and GFAP expression (n = 3/group), with β-actin as a loading control. (D)Semi-quantitative measurements of listed proteins were obtained by normalizing to β-actin. *P < 0.05 P < 0.01.

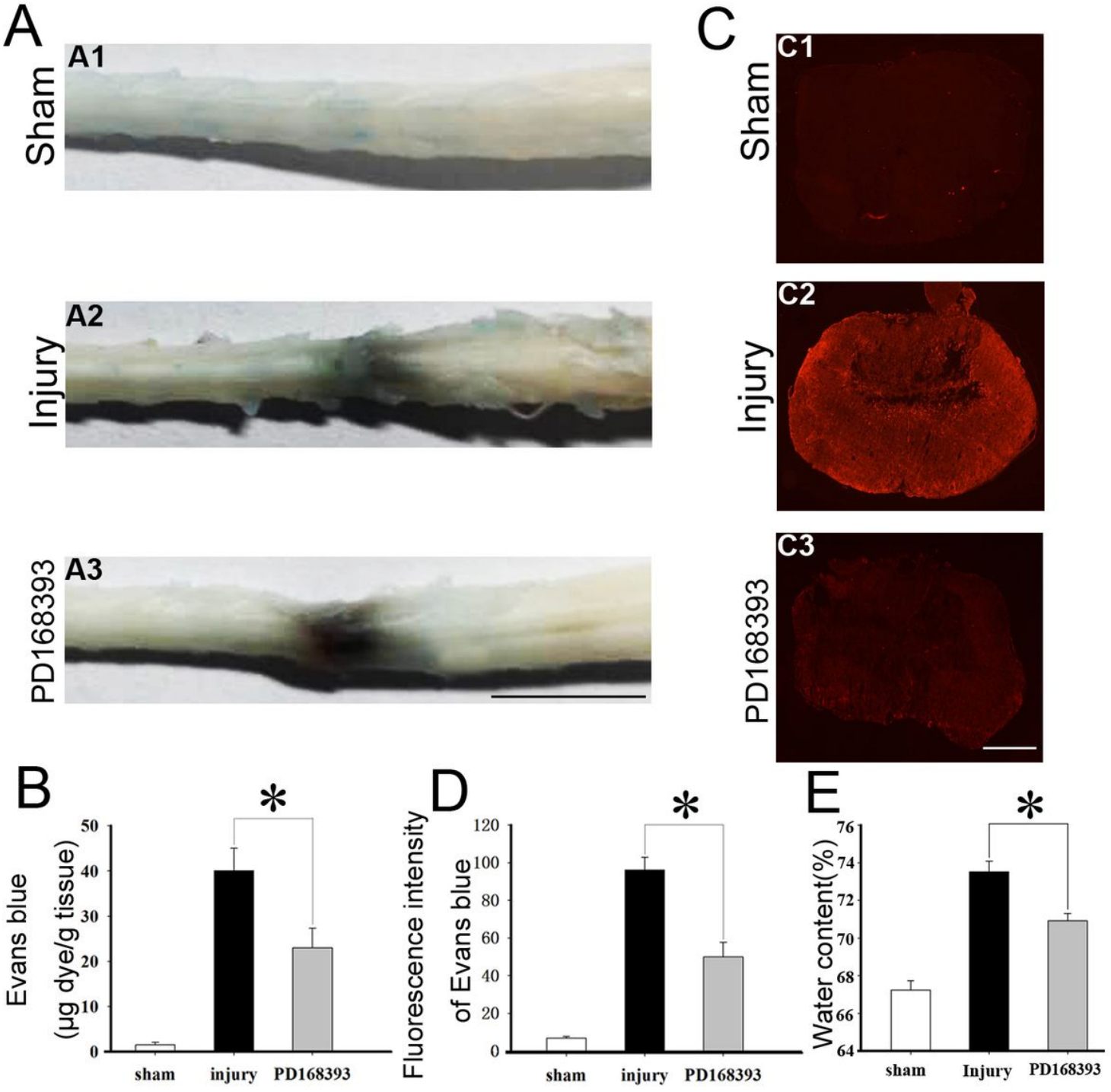

Figure 10

EGFR blockade significantly improves BSCB permeability damage after SCI. (A1-A3) are images of spinal cords in different groups rats (sham, injury, and PD168393treatment) of the Evans Blue dye extravasation experiment 3 days after SCI. Scale bars = 1 cm in A3. (B) is the analysis bar chart of Evans blue dye content in spinal cord tissues of rats in each group (Evans blue dye extravasation into spinal cord after

BSCB destruction). (C)Evans blue fluorescence images of spinal cord transverse section 1mm (rostral) near the epicenter 3 days after SCI in each group (C1, control group; C2, injury group; C3, treatment group). Scale bars =1mm in C3. (D) Statistical bar chart of Evans blue fluorescence intensity of spinal cord tissues in each group, * P < 0.05. (E) Statistical bar chart of spinal cord tissue water content in each group 5 days after spinal cord injury, * P < 0.05.

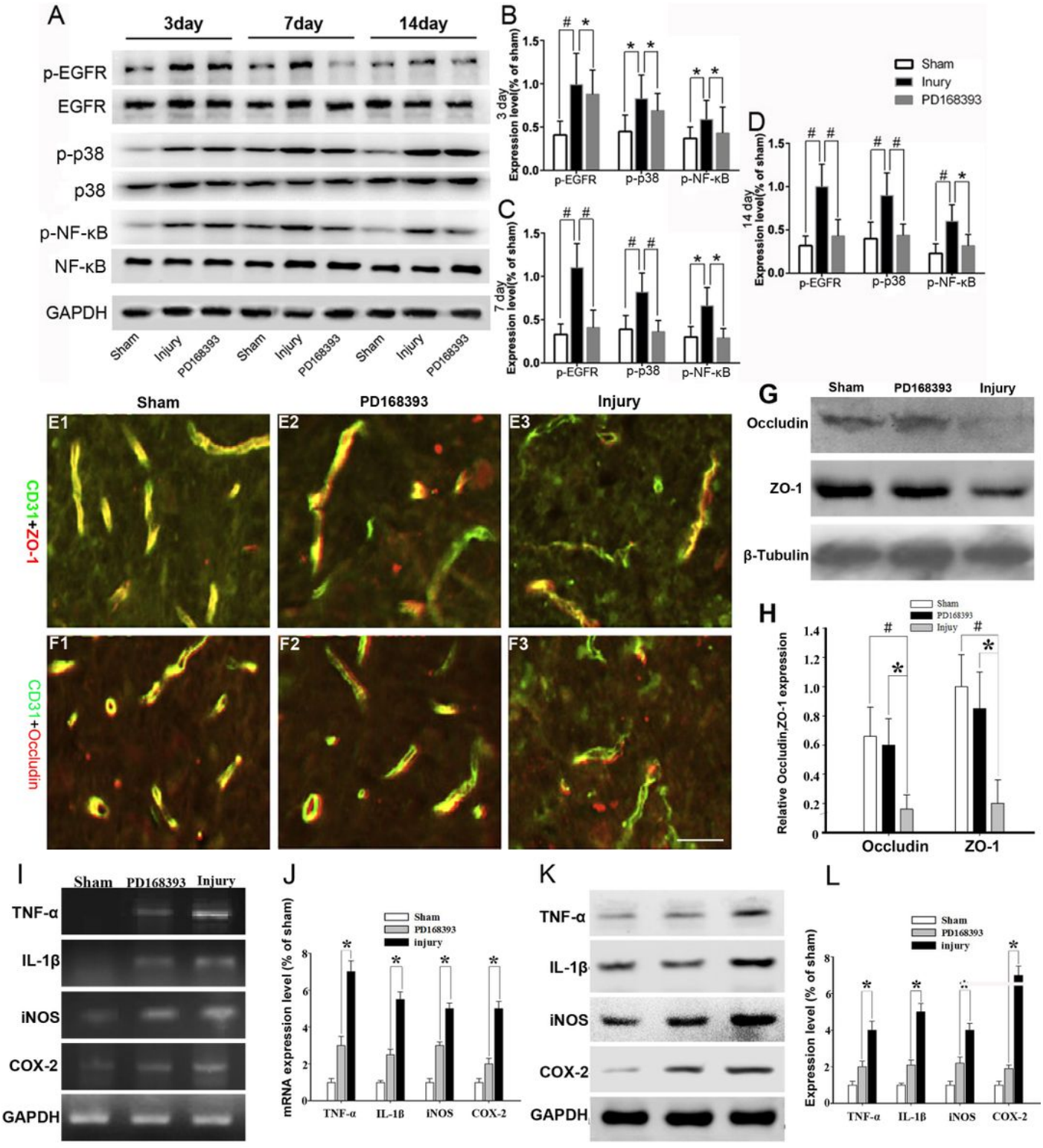

Figure 11

EGFR blockade suppresses EGFR-MAPK/NF-κB activation and alleviates TJ protein loss and cytokine production after SCI. (A-D) PD168393 (EGFR inhibitor) inhibits not only EGFR activation, but also p38 and NF-κB activation after SCI. (A) Representative Western blots of pEGFR, EGFR, p- p38, p38, p-NF-κB and NF-κB expression at different time points (3d、7d, and 14d after SC; n = 3/group), and with GAPDH as a loading control. Densitometric analysis of the pEGFR, p- p38, and p-NF-κB expression respectively at 3d (B), 7d (C) and 14d (D) after SCI, *P＜0.05、#P＜0.01. (E1-E3) Spinal cord sections were immunostained for co-localization of CD31 and ZO-1 at 3 days after SCI (n = 5/group). (F1-F3) Spinal cord sections were immunostained for co-localization of CD31 and occludin at 3 days after SCI (n = 5/group). Scale bars = 50 μm in B3 (applies to E1-F3). (G)Representative Western blots of occludin and ZO-1 expression (n = 3/group), with β-Tubulin as a loading control. (H)Semi-quantitative measurements were obtained by normalizing to β- Tubulin. *P < 0.05、P < 0.01. (I) Agarose gel electrophoretic images of TNF-α, iNOS, COX-2, and IL-1β mRNA expression of spinal cord tissue were detected by RT-PCR at day 1 after SCI. (J) statistic bar graph for the expression of TNF-α, iNOS, COX-2, and IL-1β mRNA, *P < 0.05. (K) Representative Western blots of TNF-α, iNOS, COX-2, and IL-1β expression (n = 3/group), with β-Tubulin as a loading control. (L) Semi-quantitative measurements were obtained by normalizing to β- Tubulin. *P < 0.05.

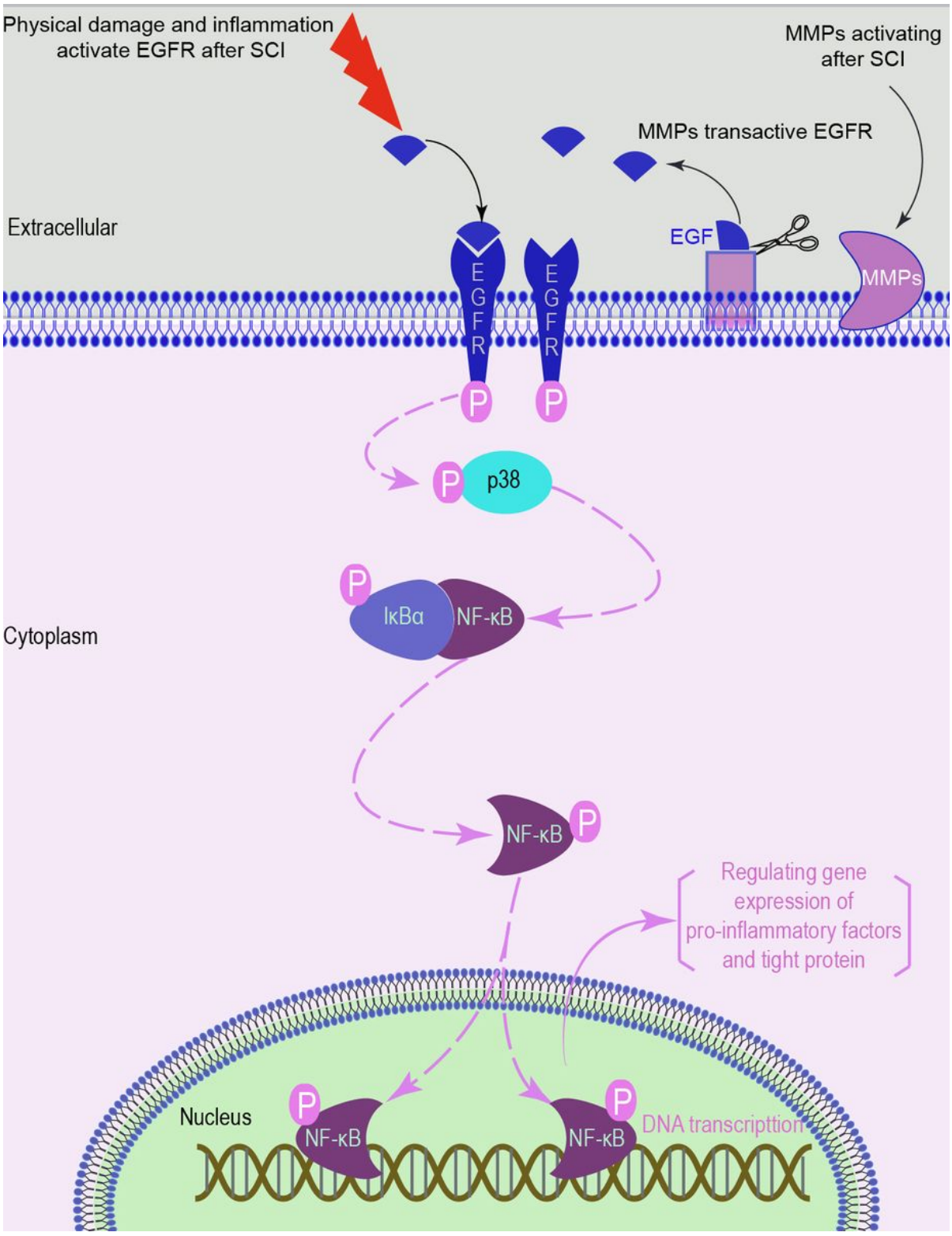

Figure 12

Schematic model showing the possible interaction between EGFR and NF- κB pathway after spinal cord injury (SCI). Physical damage and inflammation stimulation directly lead to EGFR activation (phosphorylation) or MMPs activation leads to EGFR transactivation in AS and MEC following SCI. EGFR activation leads to p38 activation (phosphorylation) which induces phosphorylation and ubiquitination of IκBα. IκBα ubiquitination leads to disintegration of IκBα and NF-κB complex and release of NF- κB.

Dissociative and activated NF-κB enters the nucleus (nuclear translocation), which activates the expression of genes such as tight junction proteins and pro-inflammatory factors.